Chapter: 1

Introduction and Literature Review

1.1 Introduction

ABO_3 type perovskite oxides (where A can be mono, di, tri and B can be di, tri, tetra, penta or hexa-valent cations) have been the topic of extensive research in theoretical as well as experimental materials science for several decades. Different categories of the perovskite materials show widely different physical properties, such as ferroelectric, piezoelectric, pyroelectric, magnetic, magnetoresistive, multiferroic etc. Perovskite is the mineral name of naturally obtained $CaTiO_3$ [Perovski (1839)]. The compounds with general formula of ABO_3 type, and having crystal structure similar to $CaTiO_3$ are classified as perovskite materials. The well known ferroelectric materials like $BaTiO_3$ [BT], $PbTiO_3$ [PT] and $PbZrO_3$ [PZ] are the simple examples of other perovskite oxide. Perovskite solid solutions $Pb(Zr_xTi_{1-x})O_3$ [PZT] [Jaffe et al. (1971)], $(1-x)Pb(Mg_{1/3}Nb_{2/3})O_3$-$xPbTiO_3$ [PMN-PT] [Singh et al. (2007)], $(1-x)Pb(Mg_{1/2}W_{1/2})O_3$-$xPbTiO_3$ [PMW-PT] [Singh et al. (2011)], $(1-x)Pb(Fe_{2/3}W_{1/3})O_3$-$xPbTiO_3$ [Mitoseriu et al. (2003)] and $(1-x)Pb(Zn_{1/3}Nb_{2/3})O_3$-$xPbTiO_3$ [PZN-PT] [Durbin et al. (1999)] etc. have attracted a lot of attention due to presence of morphotropic phase boundary (MPB) in their phase diagram which leads to maximization of physical properties in the compositions close to MPB. The maximized piezoelectric responses around the MPB make these compositions the right choice for transducer and actuator applications [Jaffe et al. (1971)]. In ferroelectric perovskite solid solutions, the morphotropic phase boundary (MPB) is nearly vertical phase boundary in the temperature composition phase diagram, where the ferroelectric and piezoelectric properties are significantly enhanced due to phase coexistence and structural instability [Jaffe et al. (1971); Singh et al. (2008)]. The perovskite lead zirconate titanate $Pb(Zr_xTi_{1-x})O_3$, abbreviated as PZT, is the most widely used piezoelectric ceramic for

sensor and actuator applications (Jaffe et al., 1971) due to its high piezoelectric response in the vicinity of a morphotropic phase boundary (MPB). However, lead is released into environment during calcinations, sintering and disposal processes of Lead-based perovskite materials, which is highly toxic and leads to cancer and other health issues [Rödel et al. (2009)]. From July, 2006, the European parliament has given directives to restrict the use or recycle of toxic materials in any kind of equipment to protect human, health and environment [Rödel et al. (2009)]. Therefore, there is a huge demand to explore the lead free perovskite materials with high T_C and high piezoelectric response. Since lead is toxic in nature therefore, these days the efforts are made towards the lead free or reduced lead based system with excellent ferroelectric and piezoelectric properties. In search of such materials currently extensive research are being done on bismuth based mixed perovskite solid solution with general formula $(1-x)Bi(M'M'')O_3$-$xPbTiO_3$ where M' and M'' are transition metal cations which are octahedrally coordinated with oxygen atom that stoichiometrically combines to give +3 charge at B-site of the perovskite structure, which shows better promises for high temperature application and good alternative of PZT. Several Bi-based piezoelectric solid solutions with reduced Pb-concentration have been explored recently such as $(1-x)BiScO_3$-$xPbTiO_3$ [Eitel et al. (2001)], $(1-x)Bi(Sc_{1/2}Fe_{1/2})O_3$-$xPbTiO_3$ [Sterianou et al. (2005)], $(1-x)Bi(Ni_{1/2}Ti_{1/2})O_3$-$xPbTiO_3$ [Choi et al. (2005)], $(1-x)Bi(Mg_{1/2}Ti_{1/2})O_3$-$xPbTiO_3$ [Randall et al. (2004), Snel et al. (2005)], $(1-x)[Bi(Mg_{3/4}W_{1/4})O_3]$-$xPbTiO_3$ [Snel et al. (2006), Stringer et al. (2005)], $(1-x)[Bi(Ni_{2/3}Nb_{1/3})O_3]$-$xPbTiO_3$ [Zhang et al. (2005)], $(1-x)(Bi_{0.7}La_{0.3})(Zn_{0.15}Mg_{0.35}Ti_{0.5})O_3$-$xPbTiO_3$ [Kobune et al. (2008)], $(1-x)BiInO_3$-$xPbTiO_3$ [Zhang et al. (2005)], $(1-x)BiMnO_3$-$xPbTiO_3$ [Woodward et al. (2004)], $(1-x)BiScO_3$-$xPbTiO_3$ [Eitel et al. (2001)], (1-

x)Bi($Ni_{1/2}Ti_{1/2}$)O_3-x$PbTiO_3$ [Pandey et al. (2014)], (1-x)Bi($Mg_{1/2}Ti_{1/2}$)O_3-x$PbTiO_3$ [Upadhyay et al. (2015)] (1-x)Bi($Mg_{1/2}Zr_{1/2}$)O_3-x$PbTiO_3$ [Pandey et al. (2014)], (1-x)$SrTiO_3$-xBi($Zn_{1/2}Ti_{1/2}$)O_3 [Pandey et al. (2013)] etc. exhibiting morphotropic phase boundary region in their phase diagram. The crystal structure of the MPB systems having disordered solid solutions have been investigated extensively [Upadhyay et al. (2015), Pandey et al. (2014)]. However, very less work has been done on the crystal structure analysis of the ordered MPB systems like (1-x)[Pb($Mg_{0.5}W_{0.5}$)O_3]-x$PbTiO_3$ [Singh et al. (2011)], (1-x)[Bi($Mg_{3/4}W_{1/4}$)O_3]-x$PbTiO_3$ [(1-x)BMW-xPT] etc., that can give an insight about the piezoelectric properties of these materials. In the present Ph.D. thesis work, we have investigated Bi-based solid solution (1-x)Bi($Mg_{3/4}W_{1/4}$)O_3-x$PbTiO_3$, which is relatively less explored for its crystal structure, phase transition behaviour and structure-property correlations. The (1-x)BMW-xPT possess high Curie temperature (T_C ~ 220^{o}C), good value of d_{33}~145pC/N, tetragonality (c/a = 1.06) and coercive field E_C ~ 42kV/cm, being more suitable for high temperature piezoelectric applications [Stringer et al. (2006); Snel et al. (2005)]. The present thesis deals with a complete study of bismuth based mixed perovskite solid solutions (1-x)Bi($Mg_{3/4}W_{1/4}$)O_3-x$PbTiO_3$ [BMW-xPT] synthesis, crystal structures, dielectric properties and nature of phase transitions. In this chapter, we briefly introduce the basic concepts and definitions of ferroelectrics and relevant topics. Then, we will present a brief review of literature on (1-x)Bi($Mg_{3/4}W_{1/4}$)O_3-x$PbTiO_3$ [BMW-xPT] solid solutions.

1.2 Perovskites Structure

Perovskite is the mineral name of calcium titanate ($CaTiO_3$). The general chemical formula for perovskite oxides is ABO_3. There can be more than one type of cations at A

and B sites in case of fractional occupancies provided they make the entire unit charge neutral and have ionic sizes which can be accommodated at these sites. The charge of 'A' and 'B' site cations combines to give +6 valences in order to balance the negative charges of the $3O^{2-}$ to maintain the charge balance and stoichiometry of perovskite structure. The ideal perovskite structure consists of a primitive cubic unit cell, where 'A' cation/cations occupy the cube corners, oxygen anion at each six faces and 'B' site cations at the centre. However, all ABO_3 compounds, which satisfy the requisite valence criterion, need not necessarily possess a stable perovskite structure. Goldschmidt in 1926 proposed tolerance factor for checking the stability of ABO_3 perovskite structure [Goldschmidt (1926)]. According to Goldschmidt the ionic radii R_A, R_B and R_O of the A, B, and O ions must have to satisfy the following relationship for the stable perovskite oxide, considering cubic closed packing of ions:

$$t = (R_A + R_O) / \sqrt{2}\,(R_B + R_O) \quad \text{..... (1.1)}$$

Where 't' is called as tolerance factor. The perovskite structure is expected to be stable if the value of 't' lies in between the range of $0.80 < t < 1.1$. The structures with $0.80 < t < 0.95$ are slightly distorted but generally non-ferroelectric (e.g. $CaTiO_3$, $SrZrO_3$), structures with $0.95 \leq t \leq 1.0$ are expected to be cubic (e.g. $SrTiO_3$) and those with $t > 1.0$ are known to show ferroelectricity (e.g. $BaTiO_3$). The symmetry is lower for the materials which have lower tolerance factors. If the value of $t > 1$ then the structure of perovskite may be tetragonal. The structure of the perovskite is expected to be rhombohedral, orthorhombic or monoclinic if the value of $t < 1$. The ideal cubic perovskite structure have *Pm*-3*m* space group, with the value of $t \sim 1$. The unit cell contains one general formula of ABO_3 and all the ions occupy special Wyckoff positions as given below:

A on 1(a) sites at 0, 0, 0

B on 1(b) sites at 1/2, 1/2, 1/2 and

O on 3(d) sites at 0, 1/2, 1/2

The A and B ions are located at the centers of cubo-octahedron and octahedron, respectively, formed by the oxygen ions. The perovskite structure can also be conveniently viewed as consisting of three-dimensional network of corner linked oxygen octahedra, with larger A-ions at the cubo-octahedral voids and the smaller B-ions filling the octahedral voids. In case of fractional occupancies of more than one type of cations at A and B-site of the perovskite structure, two different kinds of structures, namely ordered and disordered structures, may appear.

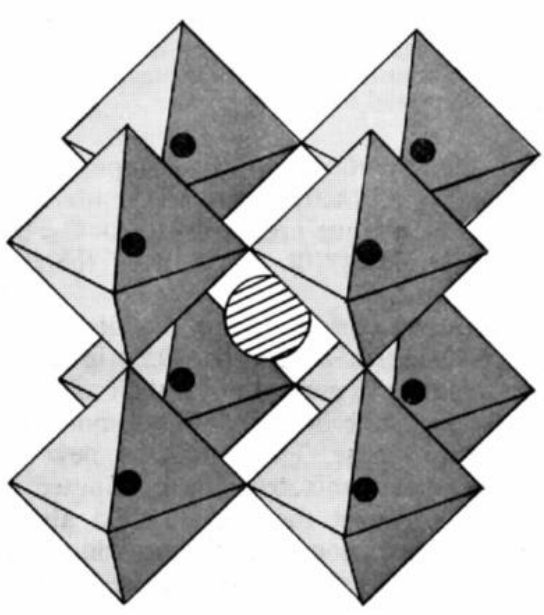

Figure 1.1 The ideal cubic (aristotype) perovskite of formula ABX_3 (A, B = cation, X = anion). The anions are at the vertices of the octahedra. Black circles B cations, hatched circle a cation [(taken from Megaw, 1973)].

1.2.1 Disordered Perovskite Structure

In case of disordered perovskite structure, the A and A' or B and B' cations have nearly similar sizes with zero or small charge differences, which leads to random distributions of these cations for the particular site in crystal lattice. Thus the unit cell for ideal cubic structure will remain primitive with the lattice parameters nearly around 3.99Å. Some examples of disordered perovskites are $Pb(Zr_xTi_{1-x})O_3$, $(Ba_xSr_{1-x})TiO_3$, [Jaffe et al. 1971] $(1-x)Pb(Fe_{1/2}Nb_{1/2})O_3$-$xPbTiO_3$, $(1-x)Pb(Fe_{2/3}W_{1/3})O_3$-$x\ PbTiO_3$ [Mitoseriua et al. (2002)], Pb_2FeNbO_6, etc.

1.2.2 Ordered Perovskite Structures

When the A-site and B-site cations are fractionally occupied by more than one type of cations having large difference in ionic sizes and charges, the ordered perovskite structure appears with the cations of different types present at alternate positions in the crystal lattices. Due to ordering in perovskite structure, the unit cell parameter is doubled for ideal cubic structure, with lattice parameter around 8Å. Several perovskites are known to exhibit cationic ordering such as Pb_2MgWO_6 [Baldinozzi et al. (1995)]; $(1-x)Pb(Mg_{1/2}W_{1/2})$-$xPbTiO_3$ [Singh et al. (2011)], Ba_2MgWO_6, Sr_2NiWO_6, Sr_2YNbO_6, $NaBaLiNiF_6$ [King and Woodward (2010)] etc. Some compounds can exhibit order-disorder transitions as a function of temperature, composition or other variables. For examples $La_{0.5}Ca_{0.5}MnO_3$ has disordered Mn^{3+} and Mn^{4+} ions at B-site at room temperature that transforms to ordered state at lower temperatures [Radaelli et al. (1997)]. The ferroelectric $Pb(Sc_{0.5}Ta_{0.5})O_3$ is also known to show order-disorder transition of B-site cations by changing temperature [Chu et al. (1993)]. Many W-based perovskites are reported to show order-disorder phase transitions such as $(1-x)Bi(Ni_{3/4}W_{1/4})O_3$-$xPbTiO_3$

[Pang et al. (2017)], (1-x)$Pb(Mg_{1/2}W_{1/2})O_3$-x$Pb(Ni_{1/3}Nb_{2/3})O_3$-x$PbTiO_3$ [Furuya et al. (1994)], $Pb(Mg_{1/3}Nb_{2/3})O_3$-$PbTiO_3$-$Pb(Mg_{1/2}W_{1/2})O_3$ [Politava et al. (2005)], Pb_2MgWO_6 [Flerov et al.(2000), Kishi et al. (1992), Seshadari et al. (1999)], Pb_2CoWO_6 [Flerov et al.(2000), Baldinozzi et al. (2000)], $NaLaMgWO_6$ [King et al. (2009)], $Pb_2Mg_{1-x}Mn_xWO_6$ [Barbur et al. (1996)], $Pb_2Mg_{1-x}Cu_xWO_6$ [Barbur et al. (2003)], $Pb(Mg_{1/3}Nb_{2/3})O_3$-$Pb(Mg_{1/2}W_{1/2})O_3$ [Gao et al. (2003), Lee et al. (1981)], $Pb_2MgW_xTe_{(1-x)}O_6$ [Rivezzi et al. (1998)] etc.

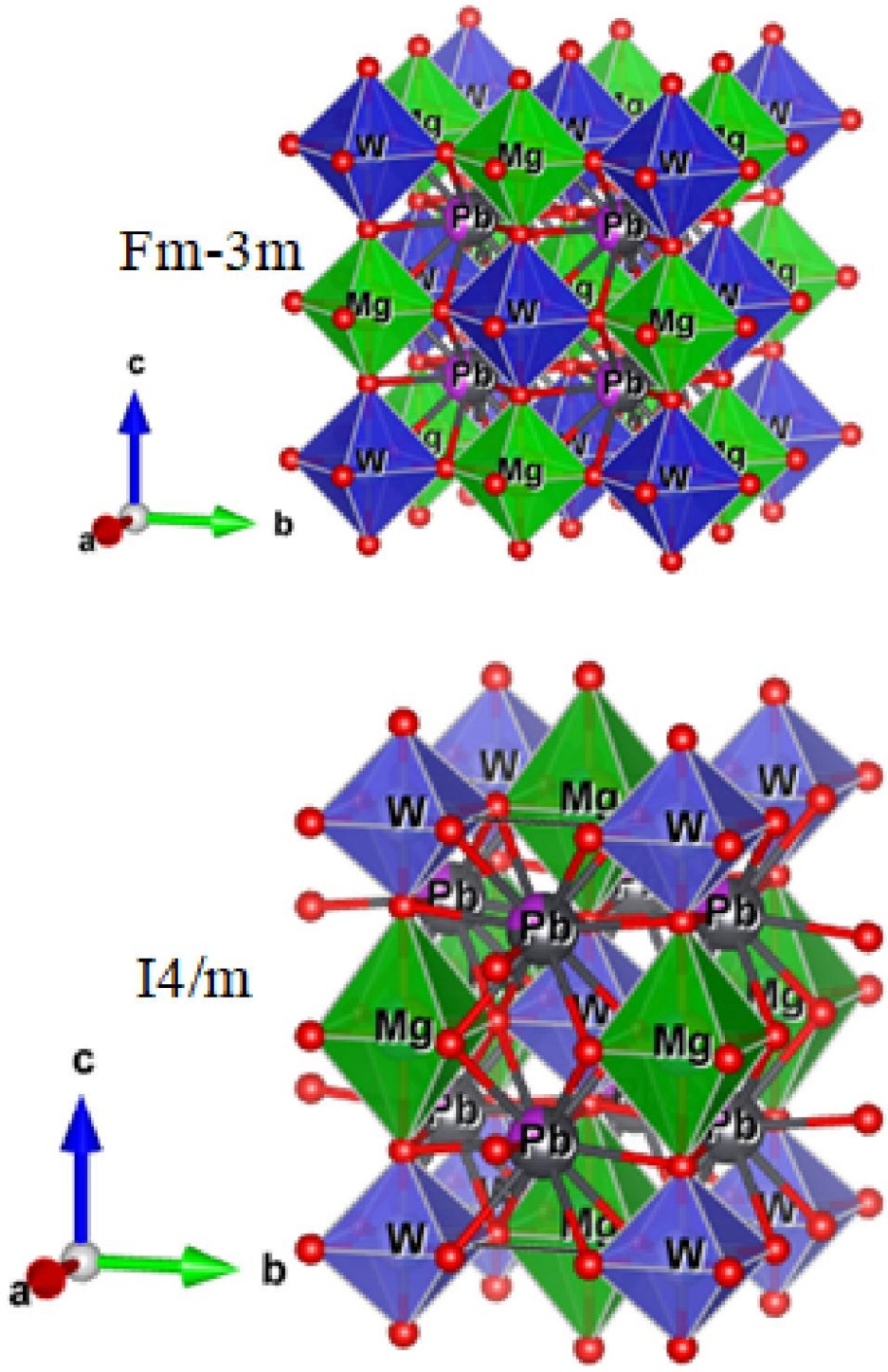

Figure 1.2 Crystal structure of the ordered cubic and ordered tetragonal perovskite of (1-x)BMW-xPT [Verma, N.K. and Singh A.K. (2019)].

.

1.3 Ferroelectric Materials

Ferroelectric materials are characterized by presence of spontaneous polarization, even in the absence of external electric field, whose direction can be reversed by the application of a suitable dc field. Under an alternating field, one observes hysteresis loop between polarization (P) and electric field (E) in a ferroelectric material similar to magnetization-magnetic field hysteresis loop of ferromagnetic materials. **Fig. 1.3** shows the typical P-E hysteresis loop for a ferroelectric material. In the absence of electric field, the polarization of ferroelectric materials converts itself into small regions of spontaneously polarized states, to minimize the energy of the system with the net macroscopic polarization zero. When external electric field is applied, the spontaneously polarized domains start to align in the direction of field hence polarization starts increasing. For sufficiently high electric fields, polarization reaches to saturation polarization (Ps) and reducing the field to zero leaves the material with some remanent polarization (Pr). Analogous to ferromagnetic materials, when the direction of field is reversed, polarization is first reduced to zero and the field required to make remanent polarization zero is called coercive field (E_C). Further higher electric field changes polarization direction as saturation polarization in the reverse direction. The Ferroelectric materials undergo a phase transition from paraelectric phase (un-polarized state) to ferroelectric phase due to development of polar axis via a crystallographic structural phase transformation at a characteristic temperature called as Curie temperature [Jaffe et al. (1971)]. Above Curie point, hysteresis loop disappears. The $BaTO_3$ possess the ferroelectric ordering and the P-E hysteresis loop at room temperature called as Curie point (T_o). The structure of $BaTO_3$ is non-centrosymmetric tetragonal with *P*4*mm* space group at room temperature. It transforms to

centrosymmetric cubic structure of paraelectric state above 130°C. In the paraelectric state, the temperature dependence of permittivity (ε') for ferroelectric materials obey the Curie-Weiss law

$$\varepsilon' = C / (T-T_C) \quad \ldots\ldots (1.2)$$

Where, 'C' and 'T_C' are Curie constant and Curie temperature respectively. The temperature above which, hysteresis loop disappears is called Curie point (T_o). In the case of a first order ferroelectric phase transformation the Curie temperature and Curie point are not identical but the Curie temperature (T_C) is lower than Curie point (T_o), while in case of second order ferroelectric phase transformation the two temperatures are identical i.e. $T_C = T_o$ [Lines and Glass (1977)]. Similar to $BaTiO_3$, $PbTiO_3$ and $KNbO_3$ also undergo ferroelectric phase transformations.

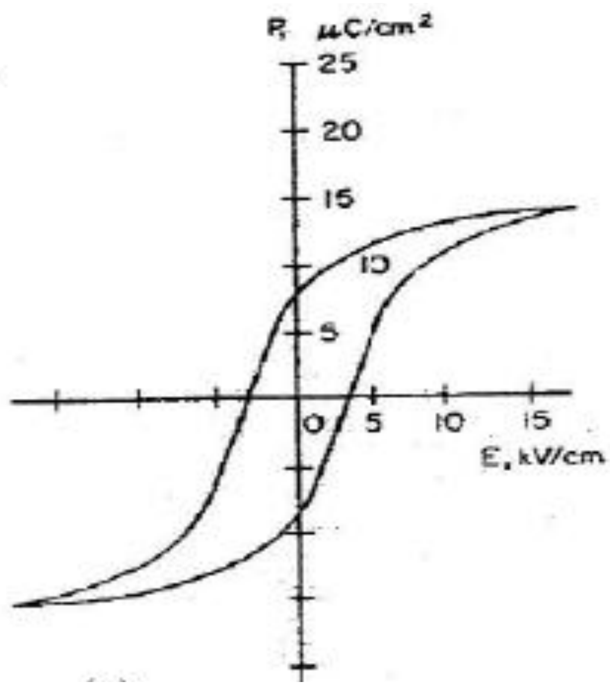

Figure 1.3 Typical P-E hysteresis loop for a ferroelectric material.

1.4 Anti-Ferroelectric Materials

Anti-ferroelectric materials have ordered dipole moments that cancel out each other completely inside each unit cell. Anti-ferroelectric materials do not have spontaneous polarization but they show sub-lattice polarization. The sufficiently high electric field can develop polarization in the anti-ferroelectric material. $NaNbO_3$ [Cross et al. (1955)] are the example of anti-ferroelectric materials. In an anti-ferroelectric phase transition, the ionic displacement occurs in equal and opposite directions in pairs. Thus the unit cell of the Anti-ferroelectric phase becomes multiple of the unit cell of the prototype paraelectric phase giving rise to the appearance of characteristic super-lattice reflections in the diffraction pattern. The transition temperature is commonly known as Neel temperature (T_N) for these materials in analogy with the Neel temperature of antiferromagnetic materials.

1.5 Relaxor-Ferroelectric Materials

Relaxor ferroelectrics or relaxors are a group of disordered crystalline materials that have peculiar structure and properties. Relaxor ferroelectrics have a diffuse and very high value of dielectric permittivity (ε) with a significant frequency relaxation in dielectric permittivity vs temperature (T) response. Relaxor ferroelectrics solid solutions have been very much interesting over the last few decades due to their superior piezoelectric properties compared to other piezoelectric ceramics. Relaxors exhibit slim polarization (P)-Electric field (E) hysteresis loop and existence of polarization above peak temperature (Tm') in the permittivity vs. temperature response. The large dielectric constants (ε), electrostrictive coefficients and electro optic constants of relaxor ferroelectrics make them ideal for super capacitors, electrostrictive actuators, biomedical transducers and optical

modulators. In contrast to relaxor ferroelectrics, the normal ferroelectrics possess well saturated polarization-electric field (P-E) hysteresis loop.

A large number of relaxors ferroelectrics are Pb-based perovskite type materials which have general formula $Pb(M_1M_2)O_3$, where M_1 have lower valence and large size cation (like Mg^{2+}, Zn^{2+}, Ni^{2+}, Fe^{3+}) and M_2 have higher valence and small size cation (like W^{6+}, Ta^{5+}, Nb^{5+}) [Cross (1987), (1994); Smolenskii (1970)]. $Pb(Mg_{1/3}Nb_{2/3})O_3$ [PMN] [Zuo-Guang Ye (2011)], $Pb(Mg_{1/3}Nb_{2/3})O_3$-$xPbTiO_3$ [PMN-PT] [Singh et al. (2007)], $Pb(Mg_{1/3}Ta_{2/3})O_3$ [Mehmet A. Akbas and Peter K. Davies (1997)], $Pb(Sc_{1/2}Ta_{1/2})O_3$ [Chu et al. (1993)], $Pb(Zn_{1/3}Nb_{2/3})O_3$ [Islam et al. (2012)], $Pb(Sc_{1/2}Nb_{1/2})O_3$ [Kojima et al. (2011)], $Pb(In_{0.5}Nb_{0.5})O_3$ [Bokov et al. (1999)], (1-x)$Pb(Zn_{1/3}Nb_{2/3})O_3$-$xPbTiO_3$ [Durbin et al. (1999)] and (1-x)$Bi(Mg_{1/2}Zr_{1/2})O_3$-$xPbTiO_3$ (BMZ-PT) [Pandey et al. (2014)] etc. are some examples of ferroelectrics which are relaxor. In general, the normal ferroelectric materials show the structural phase transformation if there is any anomaly in dielectric measurement, but in case of relaxors it is not so. The peak in real part of dielectric constant is a manifestation of the slowing down of the dipolar motion below the peak temperature (Tm) [Samara (2003)]. The temperature dependent real and imaginary parts of dielectric permittivity measured at various frequencies in a crystal of the prototypical relaxor PMN is shown in **Fig. 1.4**. The polar nano regions with randomly distributed directions of dipole moment appear below Burns temperature (TB) [Burns et al. (1983)] and the state is known as ergodic relaxor in which the polar nano regions are mobile. Above the Burns temperature the relaxors exist in non-polar paraelectric state, which is similar to paralectric state of normal ferroelectric. Around the temperatures close to TB the polar nano regions are mobile and their behaviour is ergodic. On further cooling the dynamics of polar nano

regions slows down and at the low temperature T_f, known as freezing temperature, the polar nano regions freezes into nonergodic state, while the average symmetry of the materials still remains cubic [Bokov and Ye (2006)]. The dielectric relaxation in relaxors has been classified into two categories depending on the freezing of the polar clusters.

(i) Vogel-Fulcher type behaviour [Vogel (1921); Fulcher (1925)]

(ii) Arrhenius type behaviour [Bokov et al. (2006)]

The Vogel-Fulcher type and Arrhenius type behaviour are governed by equations (1.3) and (1.4), respectively.

$$\tau = \tau_o \exp[E_a/k_B(T-T_{vf})] \quad \ldots\ldots\ldots\ldots\ldots\ldots \quad (1.3)$$

$$\tau = \tau_o \exp[E_a/k_BT] \quad \ldots\ldots\ldots\ldots\ldots\ldots\ldots\ldots \quad (1.4)$$

In the above equation, E_a is the activation energy, τ is the relaxation time, k_B is Boltzmann constant and T_{vf} is Vogal-Fulcher freezing temperature.

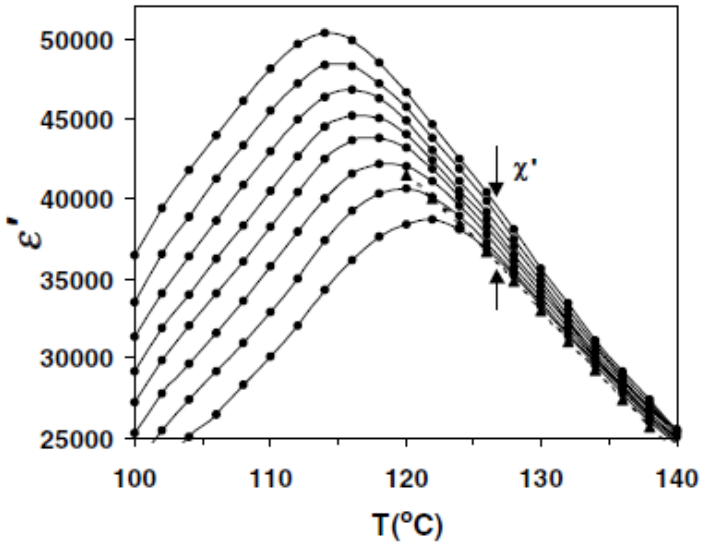

Figure 1.4 Temperature dependence of real and imaginary parts of dielectric permittivity measured at various frequencies for a crystal of the relaxor $Pb(Mg_{1/3}Nb_{2/3})O_3$ [After Bokov and Ye (2000)].

1.6 Piezoelectricity

Piezoelectricity is the capability of certain crystalline materials to generate an electric charge proportional to applied mechanical stress, discovered by Pierre and Jacques Curie brother in 1880. Piezoelectric ceramics are the materials that convert electrical energy into mechanical energy and vice versa [Curie and Curie (1880)]. The piezoelectric effects are basically of two types, one is direct piezoelectric effect and other is converse piezoelectric effect. The change in polarization by the application of stress/pressure on materials is termed as direct piezoelectric effect, and when an applied electric field physically alters the shape (strain) of materials, it is known as converse piezoelectric effect. The electrostrictive materials also develop strain on application of electric field but that is proportional to square of electric filed i.e. quadratic effect while the piezoelectric strain is directly proportional to applied electric field. The energy conversion response of piezoelectric materials is measured in terms of electromechanical coupling factor (k_P). The piezoelectric materials are very much important for the applications such as sensors, actuators, transducers used in sonar and medical ultrasound, telecommunication, aerospace and automotive industries [Jaffe et al. (1971)]. The origin of the piezoelectric effect is the displacement of cations and anions within a crystal lattice. When an external stress is applied on the materials, the ions are displaced and a net polarization is created. Thus for the appearance of piezoelectricity, the crystal structure should be polar non-centrosymmetric. The 20 crystal classes (out of 32 totals) are non-centrosymmetric crystallographic point group that show piezoelectric effect.

1.7 Morphotropic Phase Boundaries in Ferroelectric Solid Solutions

Transition from one ferroelectric to other ferroelectric phase observed due to change in composition in perovskite materials can result into a morphotropic phase transition. Such transition often leads a nearly vertical phase boundary in temperature-composition phase diagram known as morphotropic phase boundary (MPB), which separates the stability region of two crystallographically different ferroelectric phases. In other words, the morphotropic phase boundary in ferroelectric perovskite solid solutions is defined as a nearly vertical phase boundary in the temperature-composition phase diagram separating stability regions of two crystallographic phases. The coexistence of the neighboring phases and maximized dielectric, piezoelectric responses are obtained for the MPB compositions. The phase coexistence region around the MPB is known as the morphotropic phase boundary region. The structure and the properties of the perovskite solid solutions near the MPB is very sensitive to small changes in the temperature, composition etc. The composition induced phase transition in perovskite at MPB causes the instability of the polarization state, and the polarization direction can be easily rotated by an external electric field and external stress [Fu et al. (2000); Ahart et al. (2008)] resulting giant piezoelectric responses [Bellaiche et al. (2000); Noheda et al. (2001)].

Tetragonal perovskite lead titanate $PbTiO_3$ [PT] possesses large saturation polarization ($Ps \sim 81 \mu C/cm^2$) at room temperature [Jona et al. 1962] which is desirable for transducers applications. Synthesis of PT in dense ceramic form is not possible due to cubic to tetragonal phase transition and its large tetragonality (c/a = 1.064) [Jaffe et al. (1971); Subbarao (1960)] as the materials disintegrate while cooling below T_C (490ºC) after sintering. To reduce its tetragonality many efforts have been done either by chemical

substitution on Pb^{2+} and Ti^{4+} site of PT or by adding some other perovskite of type $Pb(B_1B_2)O_3$ or $Bi(B_1B_2)O_3$. Many MPB based solid solutions were developed in the effort of decreasing tetragonality of PT. Solid solutions such as $Pb(Zr_xTi_{1-x})O_3$ [Noheda et al. (2000)], $(1-x)Pb(Mg_{1/3}Nb_{2/3})O_3$-$xPbTiO_3$ [Singh et al. (2003)], $(1-x)Pb(Fe_{1/2}Nb_{1/2})O_3$-$xPbTiO_3$ [Pan et al. (2012)], $(1-x)Pb(Zn_{1/3}Nb_{2/3})O_3$-$xPbTiO_3$ [Rong et al. (2013)], $(1-x)Pb(Sc_{1/2}Nb_{2/3})O_3$-$xPbTiO_3$ [Suchomel et al. (2012)], $(1-x)Bi(Mg_{1/2}Ti_{1/2})O_3$-$xPbTiO_3$ [Randall et al. (2004)], $(1-x)Bi(Ni_{1/2}Ti_{1/2})O_3$-$xPbTiO_3$ [Pandey et al. (2014)] etc. are some examples of the MPB based piezoceramics.

1.8 Recent Developments in Solid Solutions with MPB

In PZT solid solution, it was believed that the morphotropic phase boundary separates the two crystallographic phase of rhombohedral (space group *R*3*m*) and tetragonal (space group *P*4*mm*) structure, and the coexistence of these two phases is observed around the MPB region at room temperature [Jaffe et al. (1971)]. The phase diagram and dielectric constant and planar coupling coefficient vs. composition for the PZT piezoceramics reported by Jaffe et al. (1971) is shown in **Fig. 1.5**(a) and **Fig. 1.5**(b). As can be seen from **Fig. 1.5**(a) and **Fig. 1.5**(b) the MPB separates the rhombohedral and tetragonal ferroelectric phases and the maximization of the piezoelectric responses is found around the MPB.

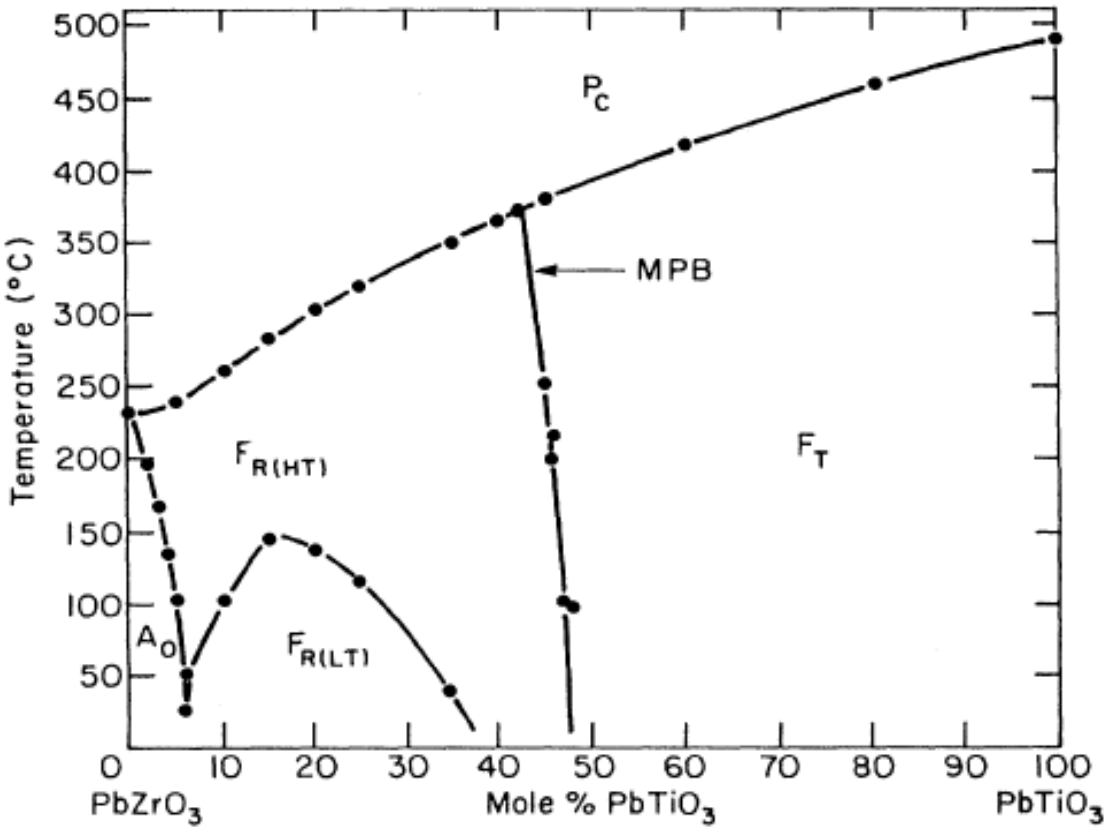

Figure 1.5 (a) Phase diagram of $Pb(Zr_xTi_{1-x})O_3$ piezoceramics [After Jaffe et al. (1971)].

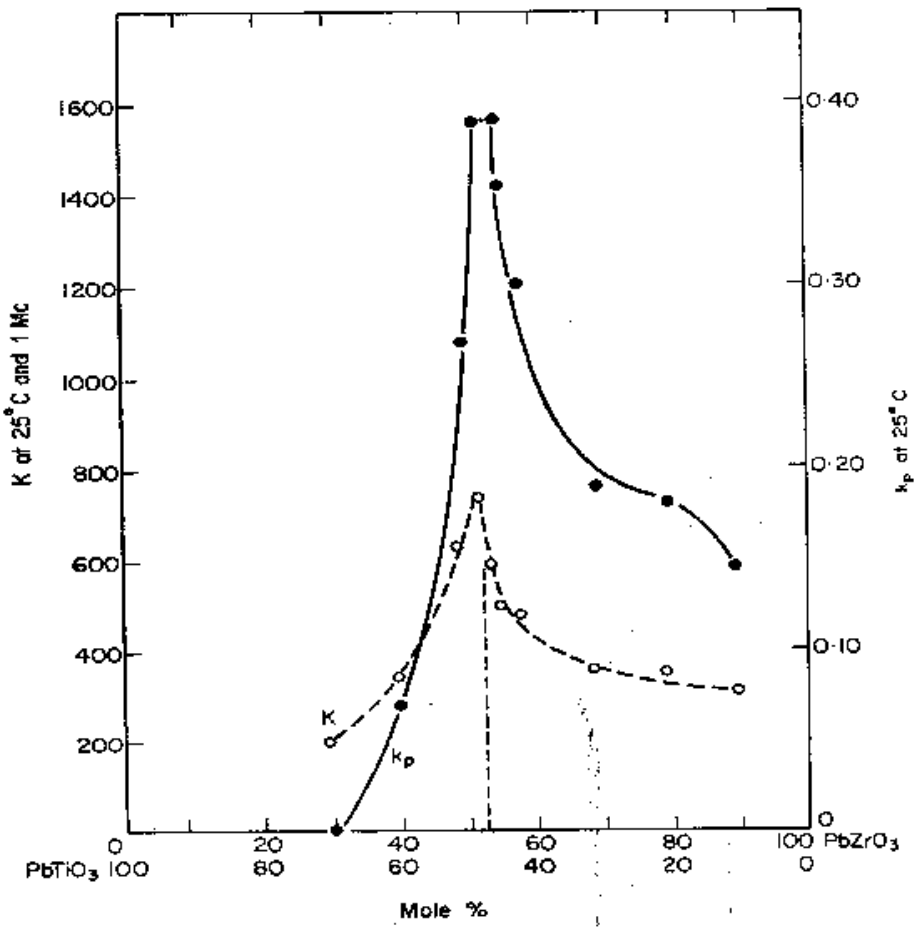

Figure 1.5 (b) Dielectric constant and planar coupling coefficient vs. composition [After Jaffe et al. (1971)].

But in past decade, presence of a monoclinic phase in the MPB region has been discovered in PZT and other MPB based solid solutions of the perovskite structure at room temperature [Fu et al. (2000); Noheda et al. (2000); Singh et al. (2003); Pandey et al. (2014)]. The phase diagram showing the presence of monoclinic phase around the MPB for the PZT and PMN-PT piezoceramics is shown **Fig. 1.6**(a,b) and **Fig. 1.7**(a) respectively. Maximization of piezoelectric strain coefficient near the morphotropic phase boundaries in (1-x)$Pb(Mg_{1/3}Nb_{2/3})O_3$-x$PbTiO_3$ is shown in **Fig. 1.7**(b). Unlike PZT, the PMN-PT system

shows two morphotropic phase boundaries [Guo et al. (2003), Singh et al (2006)]. Many other systems also show the presence of monoclinic phase around the morphotropic phase. It has been verified experimentally [Guo et al. (2000); Noheda et al. (2002)] and theoretically [Fu et al. (2000); Vanderbilt et al. (2001)] that the monoclinic phase is present near the MPB composition of the perovskite structure. In the present Ph.D. thesis, we have discovered a coexistence of Cubic (space group *Fm*-3*m*) and Tetragonal (space group *I*4/*m*) structures near the MPB composition of BMW-PT piezoceramics [Verma and Singh (2019)]. Detailed results are described in third chapter of this thesis.

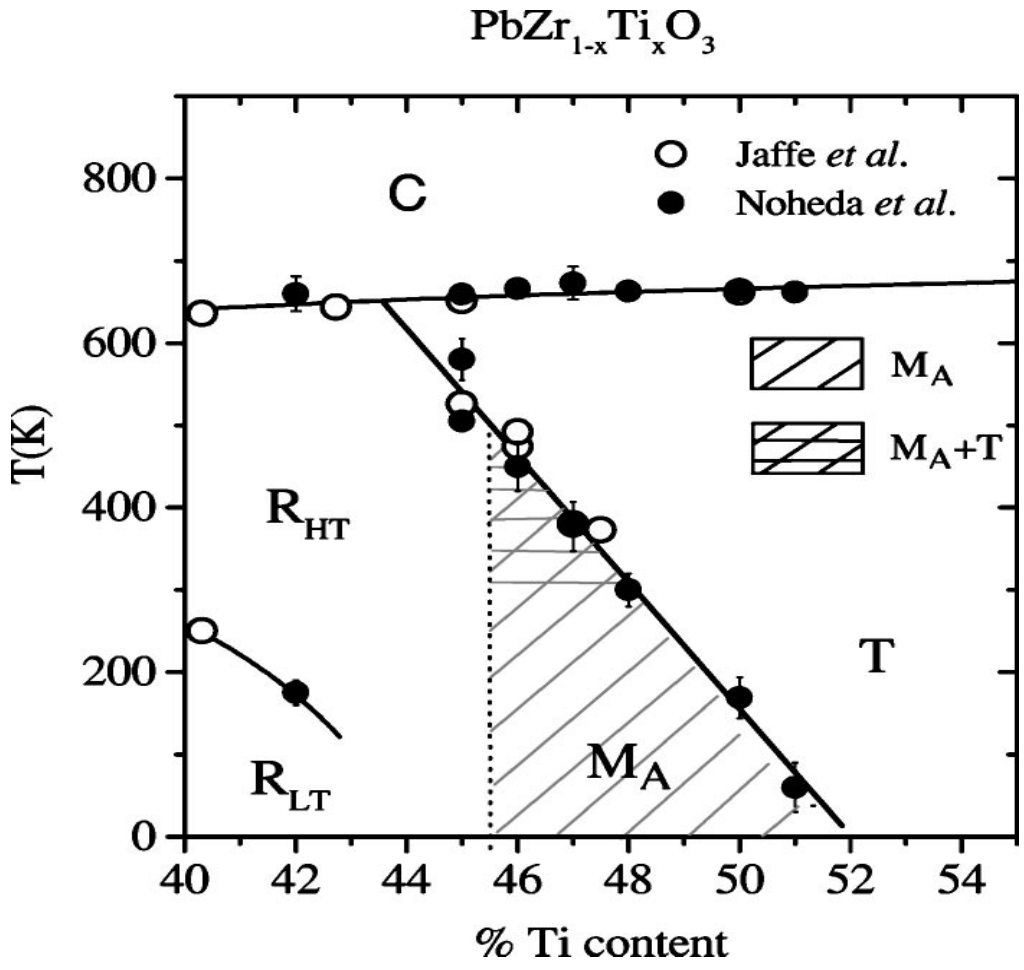

Figure 1.6 (a) Modified Phase diagram of $Pb(Zr_xTi_{1-x})O_3$ [After Noheda et al. (2002)].

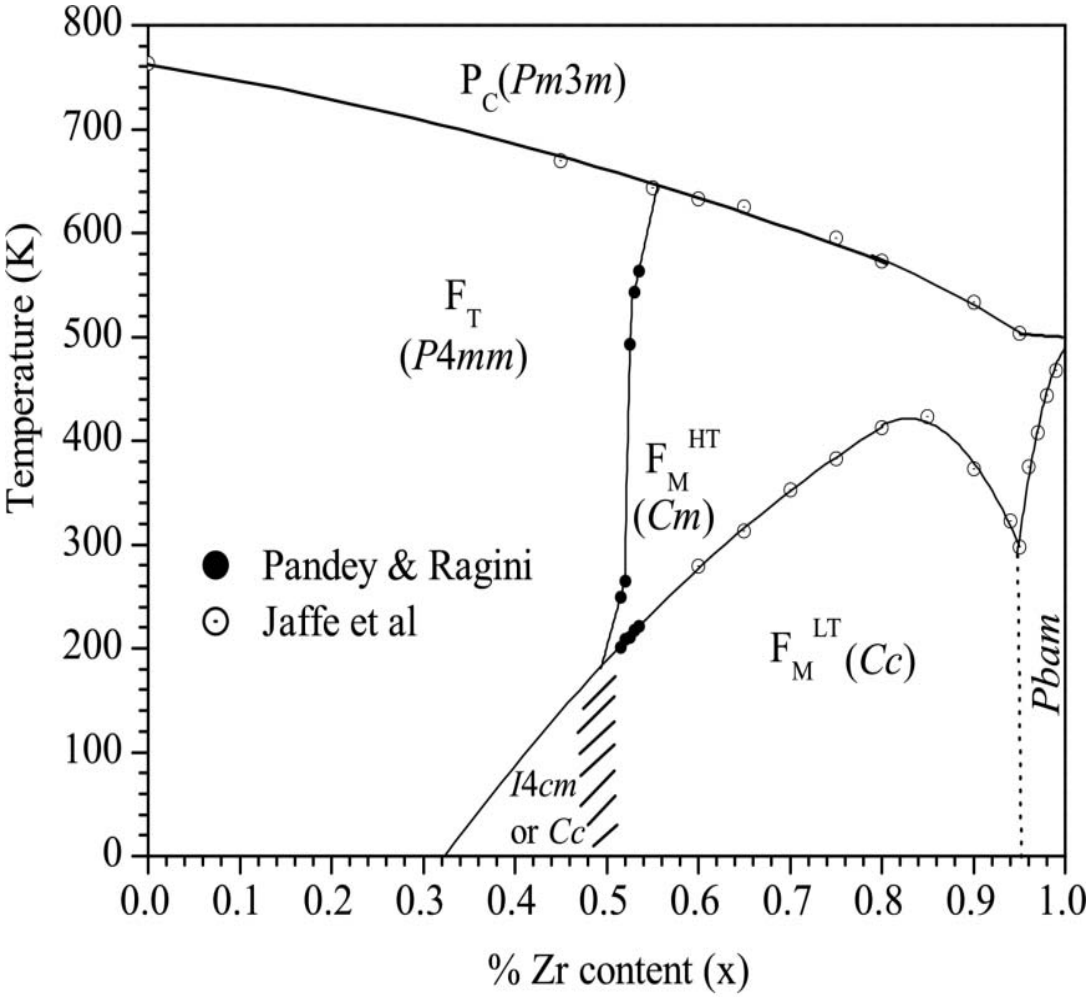

Figure 1.6 (b) Modified Phase diagram of $Pb(Zr_xTi_{1-x})O_3$ [after Pandey et al. (2008)].

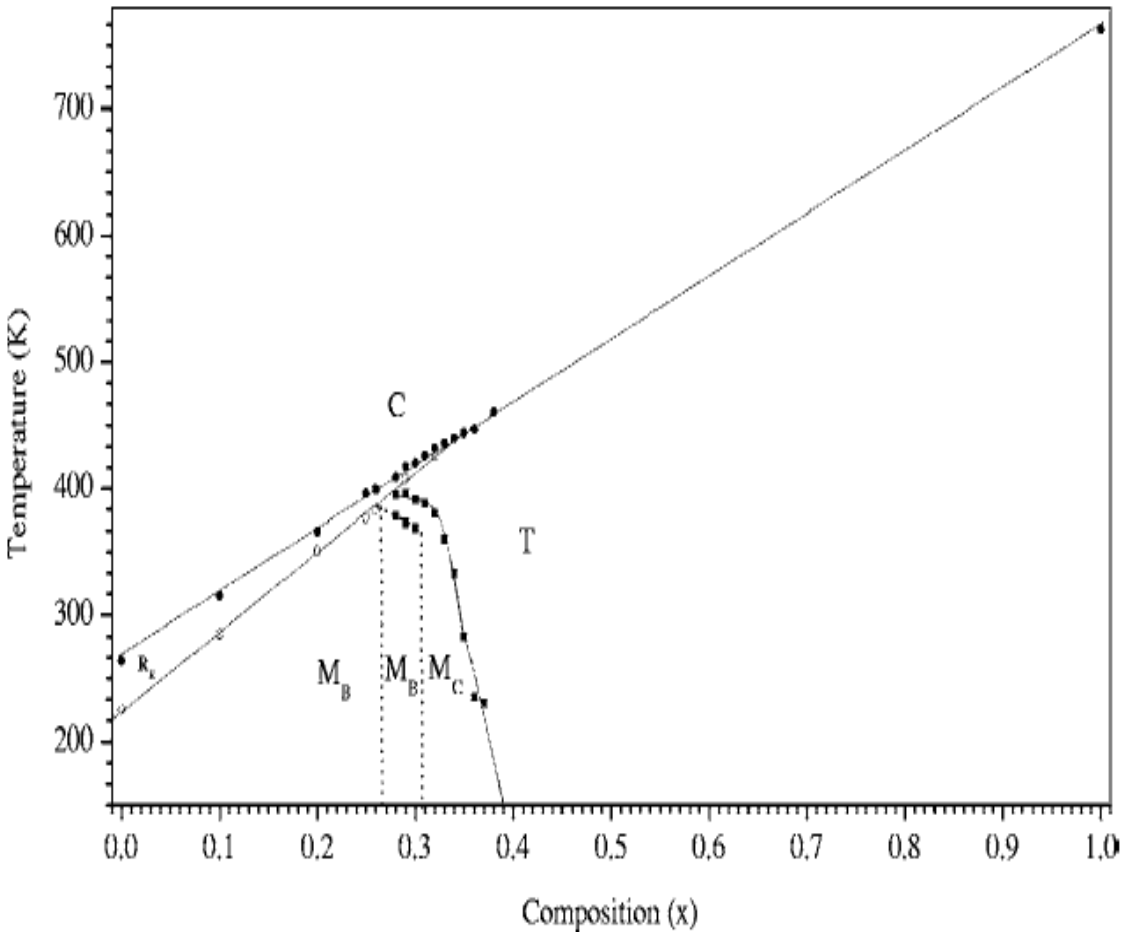

Figure 1.7 (a) Modified Phase diagram of (1-x)Pb($Mg_{1/3}Nb_{2/3}$)O_3-x$PbTiO_3$ [Singh et al. (2006)].

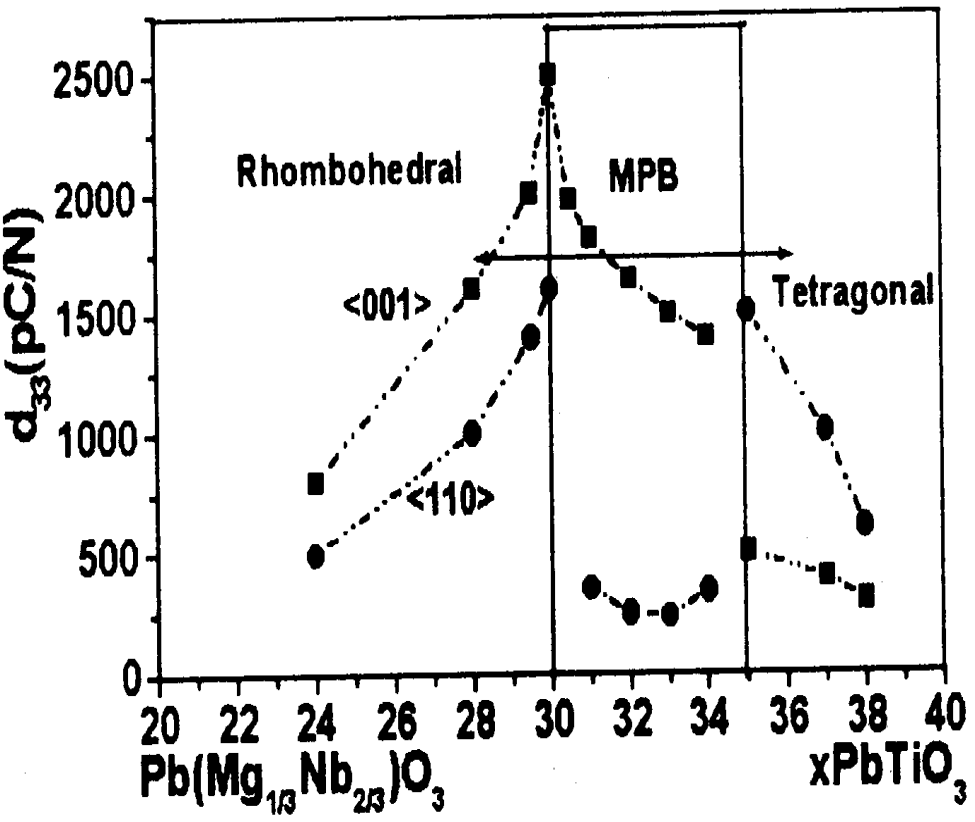

Figure 1.7 (b) Maximization of piezoelectric strain coefficient near the morphotropic phase boundaries in (1-x)$Pb(Mg_{1/3}Nb_{2/3})O_3$-x$PbTiO_3$ [After Guo et al. (2003)].

1.9 Phase Diagram of (1-x)$Pb(Mg_{1/2}W_{1/2})O_3$-x$PbTiO_3$

The phase diagram of (1-x)$Pb(Mg_{1/2}W_{1/2})O_3$-x$PbTiO_3$ solid solution shown in **Fig. 1.8** was reported for the first time by [Singh et al. (2011)] using dielectric and calorimetric data. $PbTiO_3$ has tetragonal (c/a = 1.06) structure at room temperature [Jaffe et al. (1971)] and exhibits a first-order phase transition at 495°C. After the solid solution formation of PMW with $PbTiO_3$ the paraelectric to ferroelectric phase transition temperature decreases up to 250°C for a 0.32PMW-0.68PT composition [Singh et al. (2011)]. For higher concentration of PT in PMW-xPT solid solution the transition temperature increases systematically approaches to 220^{o}C around the MPB. The phase coexistence region is

reported for the composition range $0.46 \leq x \leq 0.68$, while compositions with $x \leq 0.42$ and $x \geq 0.72$ are reported to be cubic with *Fm*3*m* space group and tetragonal with *P*4*mm* space group respectively. **Fig. 1.9** depicts the composition variation of lattice parameter and weight fraction with increasing PT concentration. Structural phase transition from pseudocubic to tetragonal phase is reported for the higher PT concentration composition with x = 0.68 [Singh et al. (2011)].

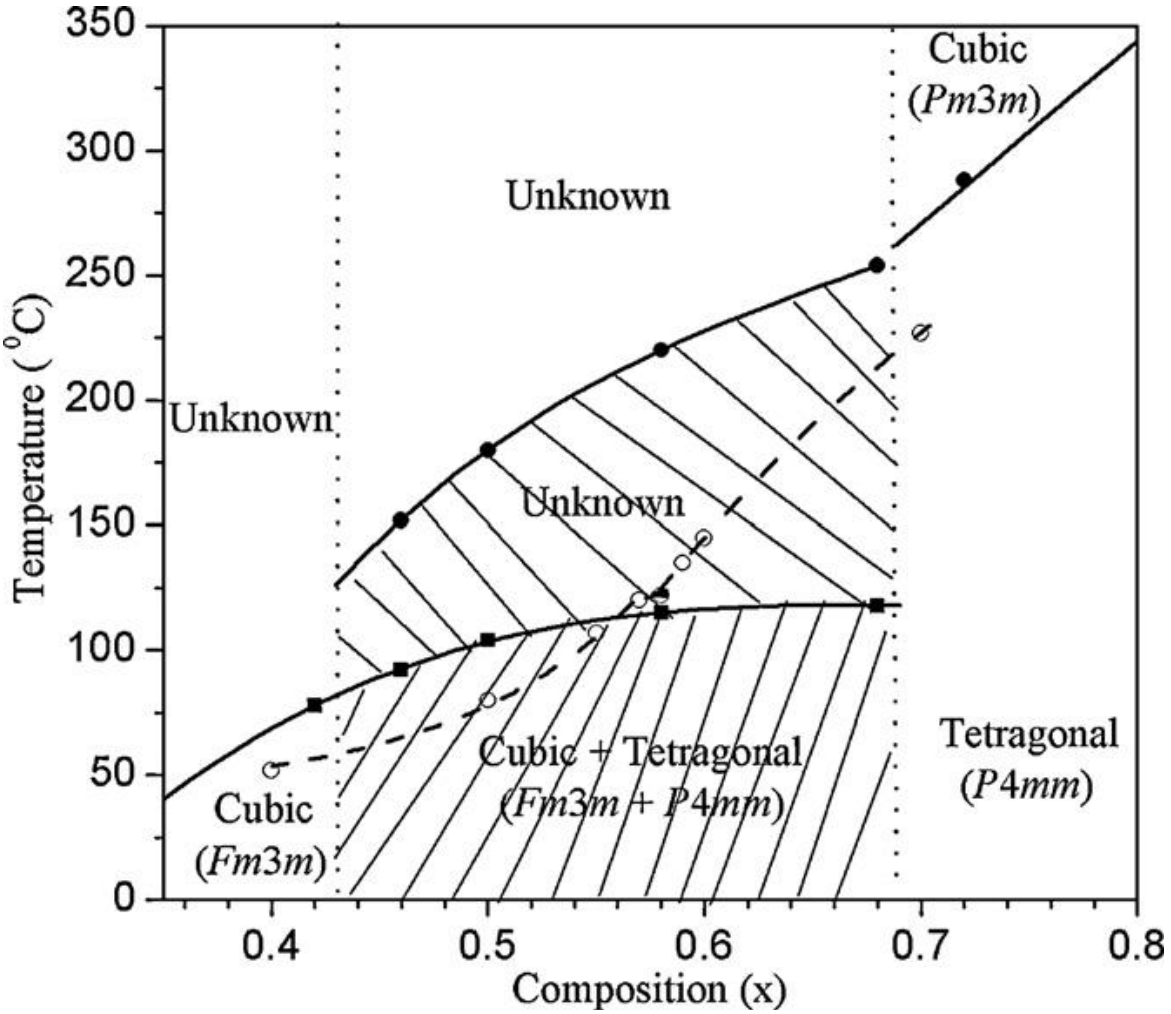

Figure 1.8 Partial Phase diagram of $(1-x)Pb(Mg_{1/2}W_{1/2})O_3$-$xPbTiO_3$ [Singh et al. (2011)].

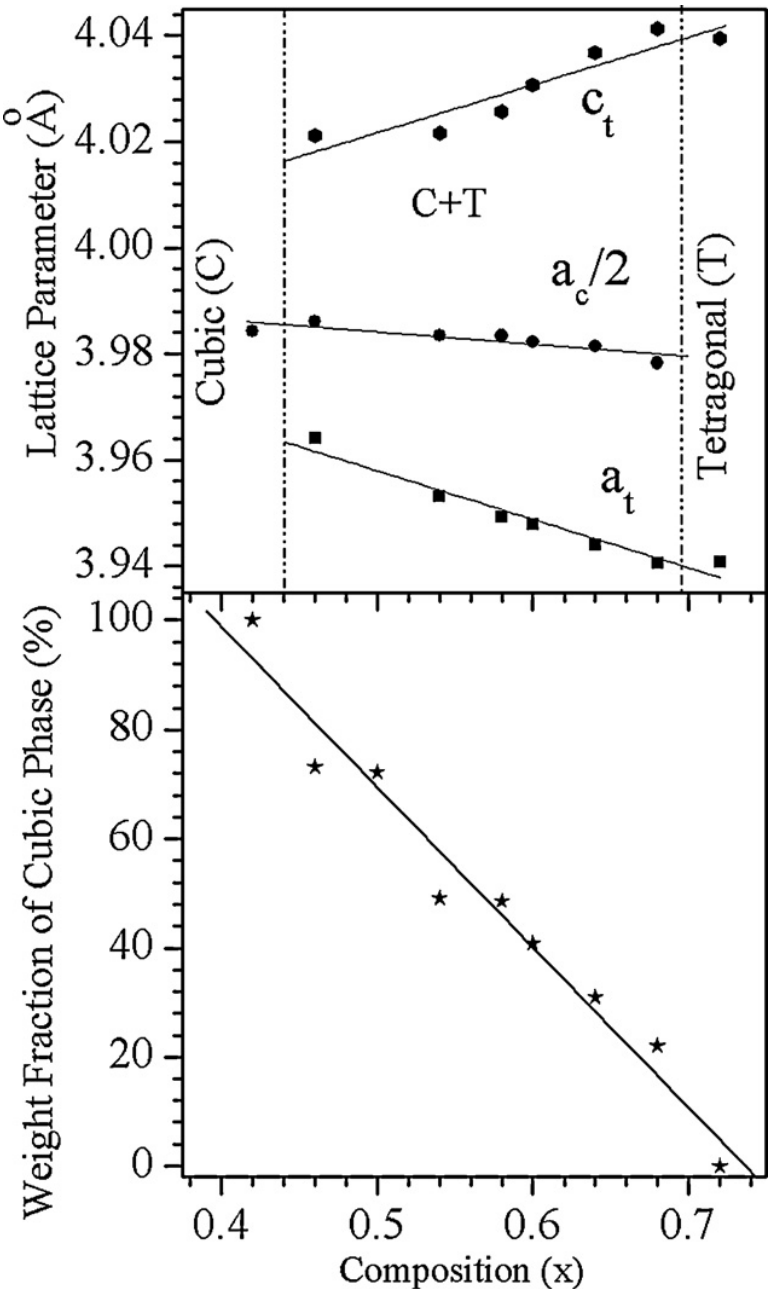

Figure 1.9 Lattice parameter and weight fraction of (1-x)Pb($Mg_{1/2}W_{1/2}$)O_3-x$PbTiO_3$ [Singh et al. (2011)].

1.10 Bi-based Perovskite Solid Solutions with MPB

Many Bi-based solid solutions are reported to show the morphotropic phase boundary between two phases such as (1-x)$Bi(Ni_{1/2}Ti_{1/2})O_3$-x$PbTiO_3$ [Pandey et al. (2014)], (1-x)$Bi(Ni_{2/3}Nb_{1/3})O_3$-x$PbTiO_3$ [Zhang et al. (2005)], (1-x)$Bi(Mg_{1/2}Ti_{1/2})O_3$-x$PbTiO_3$ [Upadhyay et al. (2014), Randall et al. (2004), Suchomel et al. (2004), Grinberg et al. (2007)], (1-x)$Bi(Mg_{1/2}Zr_{1/2})O_3$-x$PbTiO_3$ [Shabbir et al. (2007), Suchomel et al. (2004), Grinberg et al. (2007)], (1-x)$Bi(Zn_{1/2}Ti_{1/2})O_3$-x$PbTiO_3$ [Suchomel et al.(2005), Chen et al. (2007), Grinberg et al. (2007)], (1-x)$Bi(Zn_{1/2}Zr_{1/2})O_3$-x$PbTiO_3$ [BZZ-PT] [Suchomel et al. (2005), Grinberg et al. (2007)], (1-x)$Bi(Zn_{1/2}Sn_{1/2})O_3$-x$PbTiO_3$ [Suchomel et al. (2005)], (1-x)$Bi(Zn_{3/4}W_{1/4})O_3$-x$PbTiO_3$ [Chen et al. (2007), Stein et al.(2006)], (1-x)$Bi(Ni_{1/2}Hf_{1/2})O_3$-x$PbTiO_3$ [Pan et al.(2012)], x$BiMnO_3$-(1-x)$PbTiO_3$ [Castro et al. (2010)], (1-x)$BaTiO_3$-x$Bi(Mg_{0.75}W_{0.25})O_3$ [Chen et al. (2014)], (1-x)$BiFeO_3$-x$PbTiO_3$ [Bhattacharjee et al. (2007)] etc. In the following sections, we will discuss in detail the existing literature on crystal structure and dielectric behaviour of some Bi-based solid solutions e.g. (1-x)$Bi(Ni_{3/4}W_{1/4})O_3$-x$PbTiO_3$ and (1-x)$Bi(Mg_{3/4}W_{1/4})O_3$-x$PbTiO_3$ having fractional occupancy of W at B-site of the perovskite structure.

1.11 Crystal Structure and Properties of (1-x)$Bi(Ni_{3/4}W_{1/4})O_3$-x$PbTiO_3$ System

The (1-x)$Bi(Ni_{3/4}W_{1/4})O_3$-x$PbTiO_3$ [BNW-PT] solid solutions show ferroelectric behaviour. The tetragonal compositions of BNW-PT perovskite possesses large remnant polarization (Ps ~ 23.4 $\mu C/cm^2$) at room temperature [Pang et al. (2017)] which is desirable for transducers applications. Its piezoelectric coefficient is also significantly high (d_{33} ~ 145 pCN^{-1}) in morphotropic phase boundary region for the composition 0.32BNW-0.68PT. **Fig. 1.10** shows the morphotropic phase boundary between rhombohedral and tetragonal

phase for BNW-PT ceramic. The BNW-PT with compositions $x \leq 0.34$ is crystallized in rhombohedral phase and composition $x \geq 0.80$ is pure tetragonal phase. The BNW-PT has a range of Curie temperature (T_C) which varies from 460°C to ~152°C by changing the concentration of BNW. The composition dependent variation of unit cell parameters (a & c) for BNW-PT is depicted in **Fig. 1.11**(a) and the tetragonality (c/a) which decreases with increasing PT concentration is shown in **Fig. 1.11**(b).

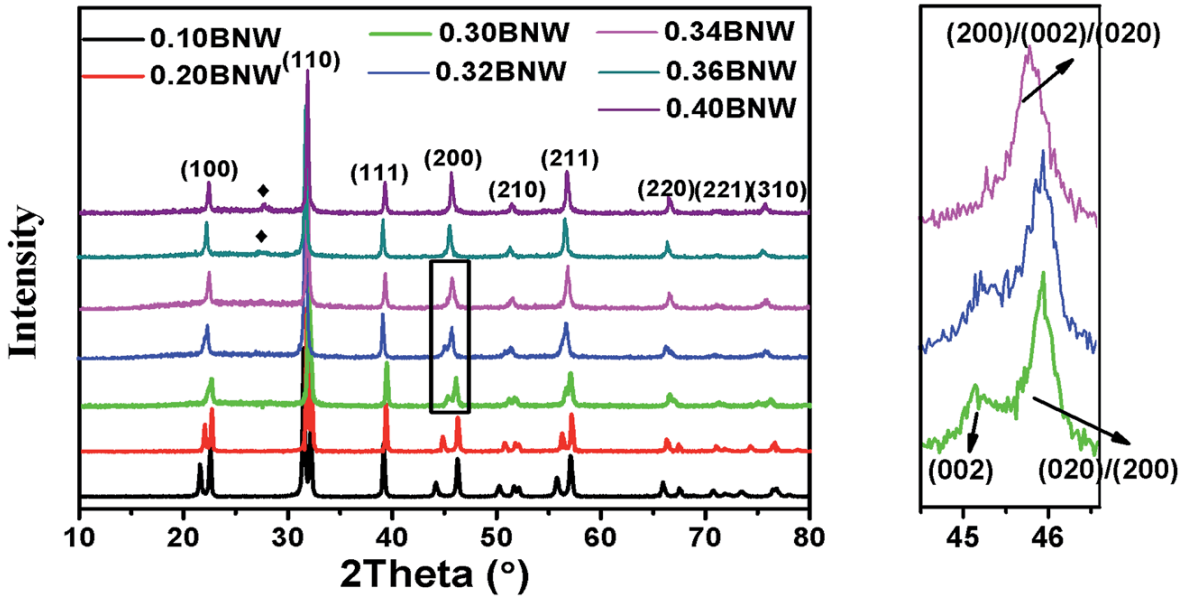

Figure 1.10 Powder X-ray diffraction patterns of xBNW-(1-x)PT ceramics with x = 0.1-0.4 (left); the enlarged XRD profiles of (200) reflections for MPB compositions (right) [Pang et al. (2017)].

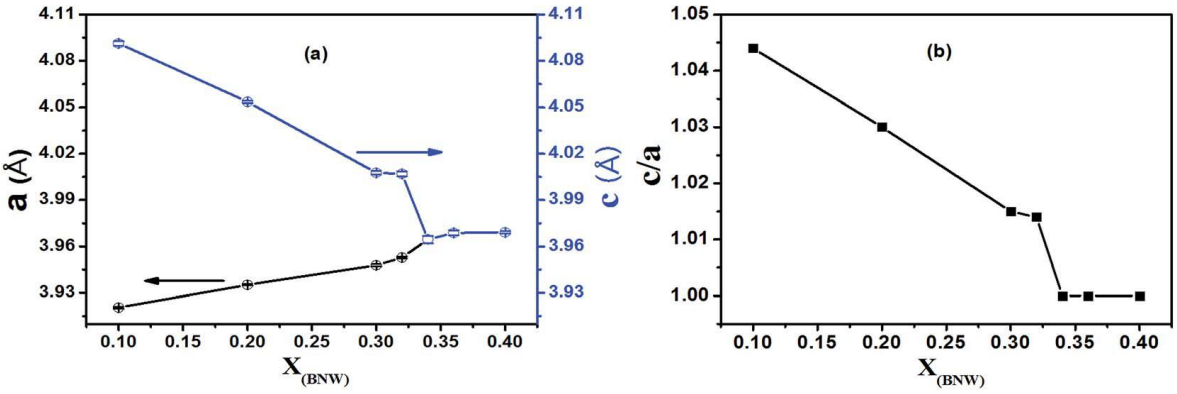

Fig 1.11 (a) The unit cell parameters a, c for various compositions; (b) the tetragonality c/a for various compositions [Pang et al. (2017)].

1.12 Dielectric Properties of (1-x)Bi($Ni_{3/4}W_{1/4}$)O_3-x$PbTiO_3$ System

The temperature dependent dielectric permittivity and dielectric loss measured at various frequencies for (1-x)Bi($Ni_{3/4}W_{1/4}$)O_3-x$PbTiO_3$ system reported by et al.(2017) is shown in **Fig. 1.12**. The ferroelectric to paraelectric phase transition varies with composition and the Curie temperature at MPB region is approximately 220°C.

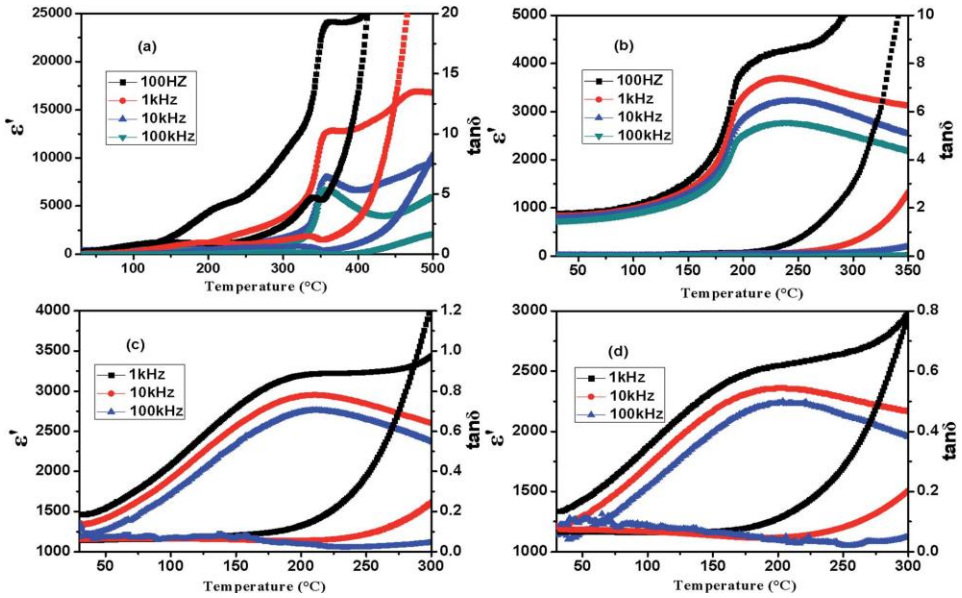

Figure 1.12 Temperature dependence of dielectric permittivity and dielectric loss for xBNW-(1-x)PT ceramics: (a) x = 0.20 (b) x = 0.30 (c) x = 0.34 (d) x = 0.36 [Pang et al.(2017)].

1.13 The (1-x)Bi($Mg_{3/4}W_{1/4}$)O_3-x$PbTiO_3$ Solid Solution System

The (1-x)Bi($Mg_{3/4}W_{1/4}$)O_3-x$PbTiO_3$ [BMW-xPT] solid solution is also a high temperature piezoelectric material, which can be useful for actuators and transducers for space technology and automotive industries etc [Qureshi et al. (2007)]. In this case also, the preparation of Bi($Mg_{3/4}W_{1/4}$)O_3 in pure perovskite form of ceramics is not possible due to less stable perovskite phase because of lower tolerance factor. Solid solution formation with $PbTiO_3$ stabilizes the perovskite phase. The XRD analysis of sintered samples for lower concentrations of $PbTiO_3$ shows impurity phase of Bi_2WO_6 [Khalyavin et al. (2006)]. In case of (1-x)BMW-xPT the paraelectric to ferroelectric phase transition near MPB compositions occurs around ~300°C. The room temperature reported value of the remnant polarization (P_r) and coercive field (E_C) are ~29μC/cm^2 and ~23kV/cm, respectively [Qureshi et al. (2007)]. BMW-PT shows the high dielectric constant value ~1387 at room temperature near the morphotropic phase boundary region [Qureshi et al. (2007)].

1.14 The Reported Crystal Structure of (1-x)Bi($Mg_{3/4}W_{1/4}$)O_3-x$PbTiO_3$ Ceramics

The x-ray diffraction patterns of (1-x)Bi($Mg_{3/4}W_{1/4}$)O_3-x$PbTiO_3$ [BMW-xPT] ceramic for x = 0.50, 0.62 and 0.70 compositions reported by [Snel et al. (2006)] are shown in **Fig. 1.13** (A), (B) and (C) respectively. The crystal structure corresponding to x = 0.50, 0.62 and 0.70 compositions are reported to be rhombohedral, pure tetragonal and the coexistence of rhombohedral and tetragonal phases respectively.

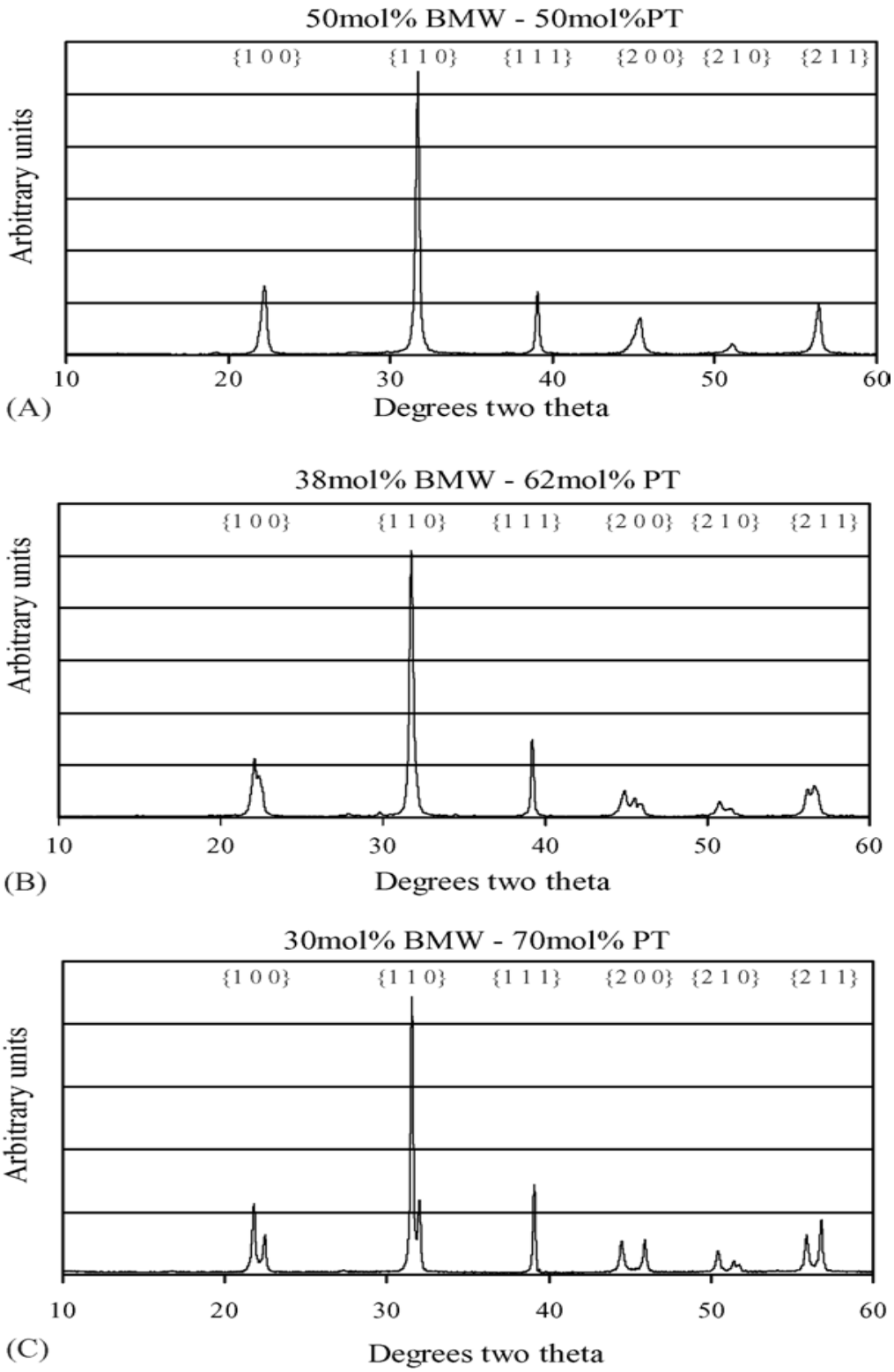

Figure 1.13 XRD pattern of (1-x)Bi($Mg_{3/4}W_{1/4}$)O_3-x$PbTiO_3$ [After Snel et al. (2006)].

1.15 Old Phase Diagram of (1-x)$Bi(Mg_{3/4}W_{1/4})O_3$-x$PbTiO_3$

The composition dependent variation of lattice parameters with increasing PT concentration and phase coexistence region in the composition range $0.45 \leq x \leq 0.52$ reported by Stringer et al. (2005)] is depicted in **Fig.1.14**. Structural phase transition from pseudocubic rhombohedral to tetragonal phase is reported around the composition with x=0.62 [Stringer et al. (2005)]. The phase coexistence MPB region is not well characterized by these authors.

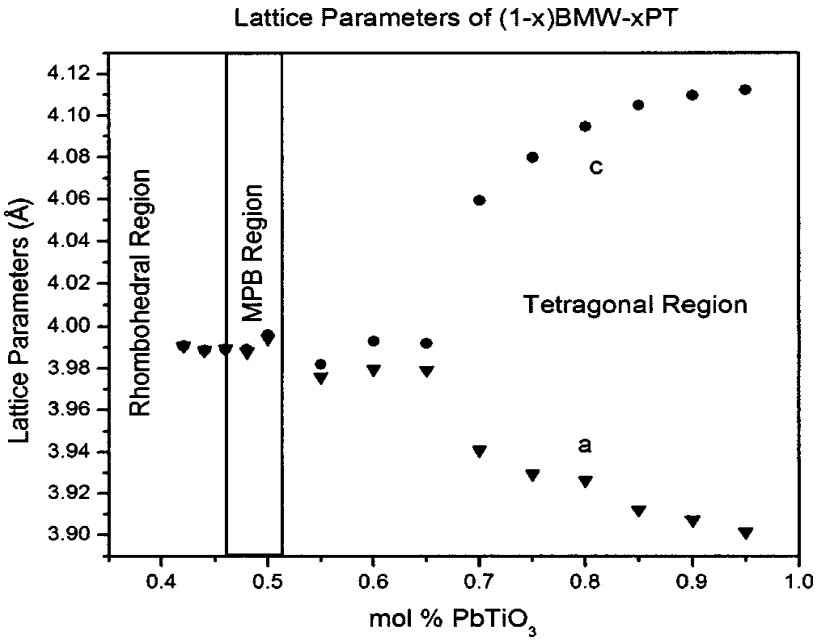

Figure 1.14 Composition dependence of lattice parameters for (1-x)$Bi(Mg_{3/4}W_{1/4})O_3$-x$PbTiO_3$ reported by Stringer et al. (2005).

The phase diagram of (1-x)$Bi(Mg_{3/4}W_{1/4})O_3$-x$PbTiO_3$ solid solution was at first reported by Stringer et al. (2005) using dielectric and calorimetric data and is shown in **Fig. 1.15**. The $PbTiO_3$ has tetragonal (c/a = 1.06) structure at room temperature [Jaffe et al. (1971)] and exhibits a first-order phase transition at 490^oC. After the solid solution formation of $Bi(Mg_{3/4}W_{1/4})O_3$ with $PbTiO_3$ the paraelectric ferroelectric transition

temperature decreases up to 145°C for a 0.55BMW-0.45PT composition [Stringer et al. (2005)]. For higher concentrations of $PbTiO_3$ in (1-x)Bi($Mg_{3/4}W_{1/4}$)O_3-x$PbTiO_3$ solid solution the transition temperature increases systematically and approaches to 220^oC around the MPB as reported by Stringer et al. (2005). The MPB region is reported to lie around x = 0.50 composition. As discussed in Chapter 3 of the present thesis, the correct crystal structures and the location of the MPB region in (1-x)Bi($Mg_{3/4}W_{1/4}$)O_3-x$PbTiO_3$ is completely different from those reported by earlier authors.

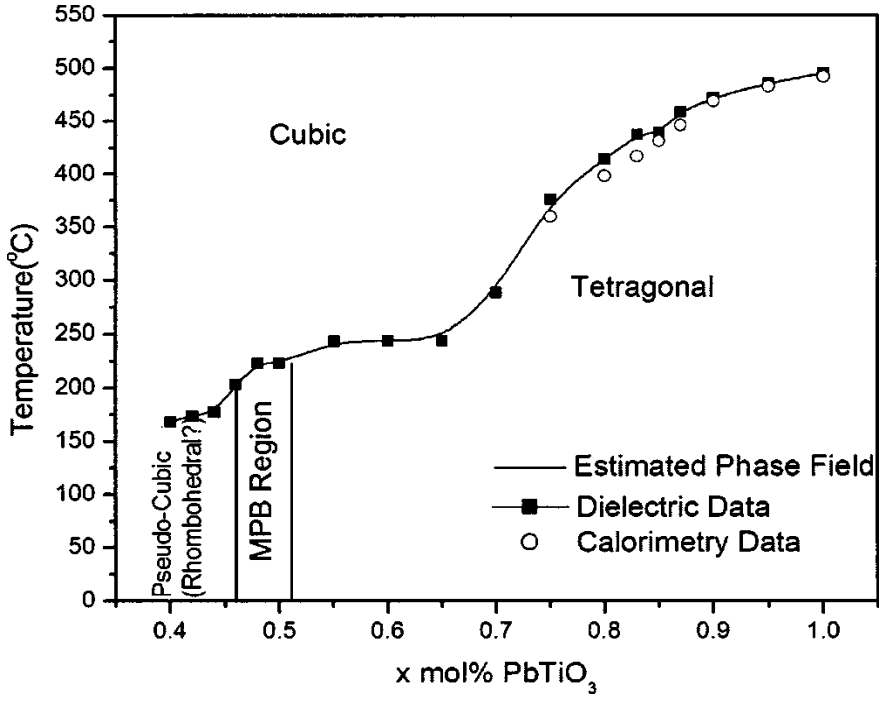

Figure 1.15 Phase diagram of (1-x)Bi($Mg_{3/4}W_{1/4}$)O_3-x$PbTiO_3$ reported by Stringer et al. (2005).

1.16 Electric Field Induced Phase Transitions in Some Bi-based System

Electric field induced structural changes has been investigated in several MPB systems such as such as $PbZr_{1-x}Ti_xO_3$ [Schönau et al. (2007), Guo, et al. (2000)], (1-x)$Pb(Mg_{1\backslash3}Nb_{2\backslash3})O_3$-x$PbTiO_3$ [Park et al. (1997), [Bokov et al. (2008), Guo et al. (2002)], 0.67$Pb(Mg_{1/3}Nb_{2/3})O_3$-0.33$PbTiO_3$ [Zheng et al. (2015)], 0.68$Pb(Mg_{1/3}Nb_{2/3})O_3$-0.32$PbTiO_3$ [PMN-0.32PT] [Li et al. (2008)], (1-x)$Pb(Zn_{1\backslash3}Nb_{2\backslash3})O_3$-x$PbTiO_3$ [Uchino et al. (2000); Noheda et al. (2001)], (Pb, La)(Zr, Sn,Ti)O_3 [Gao et al. (2015)]. Electric field induced phase transitions have been reported recently in several Bi-based MPB systems also such as (1-x)$Bi(Ni_{1/2}Ti_{1/2})O_3$-x$PbTiO_3$ [Pandey and Singh (2014)], (1-x)$Bi(Mg_{1/2}Ti_{1/2})O_3$-x$PbTiO_3$ [Upadhyay and Singh (2016)], (1-x)$Bi(Mg_{1/2}Zr_{1/2})O_3$-x$PbTiO_3$ [Upadhyay et al. (2017].

Evolution of the pseudocubic (111), (200) and (220) XRD peak profiles for the MPB composition 0.42$Bi(Mg_{1/2}Zr_{1/2})O_3$-0.58$PbTiO_3$ system poled at different electric field such as 10, 20 and 30kV/cm reported by Upadhyay et al. (2017) is shown in **Fig. 1.16**. The XRD profile peak corresponding to unpoled sample (bottom profile in **Fig. 1.16**) shows the coexistence of cubic and tetragonal structures. After electric field poling the structure transforms into tetragonal phase as is evident from the tetragonal splitting of the diffraction profiles shown in **Fig. 1.16**. It can be easily seen that the intensity of (002) profile is enhanced drastically with the increase in the poling field strength. This indicates that an enhancement in the poling field strength transforms the coexisting cubic phase of the unpoled ceramic (bottom profile in **Fig. 1.16**) to tetragonal phase. In the present Ph.D. thesis also, we report a similar electric field induced phase transition in (1-x)$Bi(Mg_{3/4}W_{1/4})O_3$-x$PbTiO_3$ ceramic and the results are described in Chapter 5.

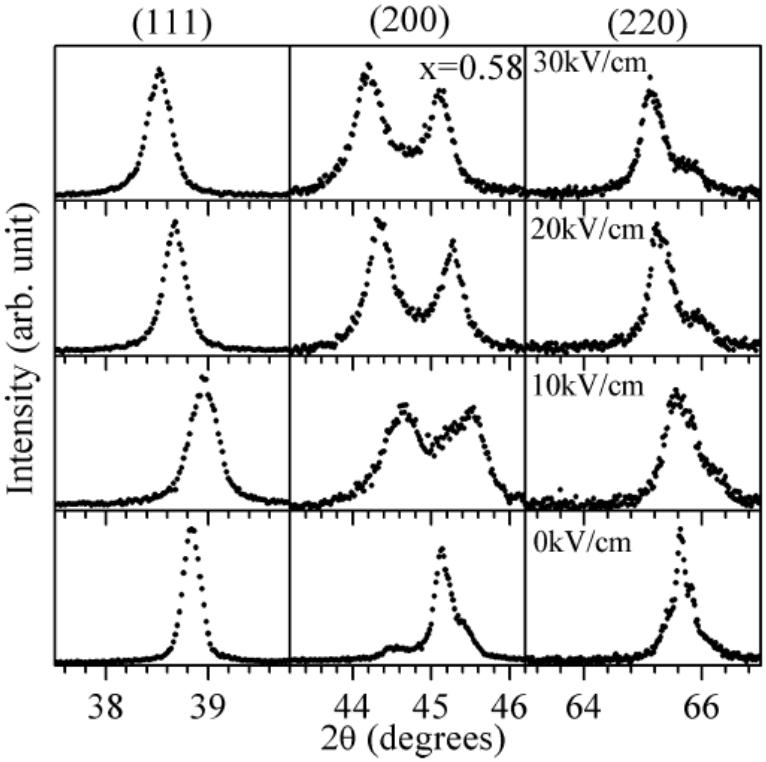

Figure 1.16 Evolution of the pseudocubic (111), (200) and (220) XRD profiles for $0.42Bi(Mg_{1/2}Zr_{1/2})O_3$-$0.58PbTiO_3$ ceramics electrically poled at various field strengths [After Upadhyay et al. (2017)].

Fig. 1.17 shows the variation of lattice parameters of poled (at 30 kV/cm) and unpoled $(1-x)Bi(Mg_{1/2}Zr_{1/2})O_3$-$xPbTiO_3$ piezoceramics for compositions x = 0.55, 0.58 and 0.61 reported by Upadhyay et al. (2017). The lattice parameters are observed to get modified due to electric field poling. Thus the crystal structure and phase stability of the poled sample differs significantly from that of the un-poled samples. This highlights the importance of investigating crystal structure of the MPB ceramics after electric field poling.

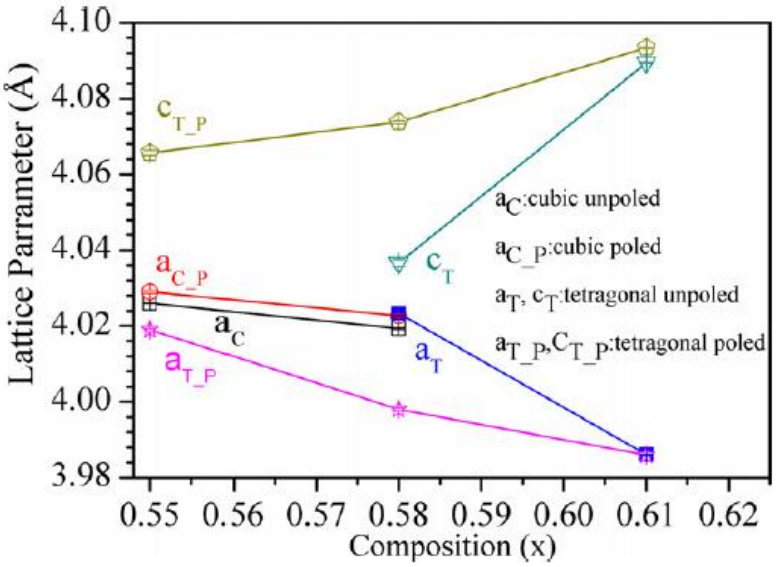

Figure 1.17 Variation of lattice parameters with composition (x) of (1-x)Bi($Mg_{1/2}Zr_{1/2}$)O_3-x$PbTiO_3$ piezoceramics poled at an electric field of 30kV/cm along with the unpoled sample [Upadhyay et al. (2017)].

1.17 Effect of Grain Size on the Crystal Structure and Phase Coexistence in MPB Ceramics

There is significant literature on the modifications of the crystal structure, polarization, dielectric and phase transition behaviour of ferroelectric ceramics by decreasing grain size [Duiker and Beale (1990], Frey and Payne, (1996), Hornebecq et al. (2004), Zhao et al. (2004), Curecheriu et al. (2012), Ghosh et al. (2014), Benabdallah et al. (2015)], Tan et al. (2015)], Muthuramalingam et al. (2016)], Khatua et al. (2017)], Koruza et al. (2017)]. It is reported that the monoclinc lattice distortion of $Na_{0.5}Bi_{0.5}TiO_3$ disappears by decreasing grain size to ~2.5 μm and below [Khatua et al. (2017)]. In tetragonal compositions close to MPB for (1-x)$BiFeO_3$-x$PbTiO_3$ ceramic the pure tetragonal phase is reported to transform into coexisting tetragonal and rhombohedral

structures when the average crystallite size is reduced from 10 μm to1 μm [Kothai et al. (2014)]. Similarly, for the MPB compositions of (1-x)$Bi(Mg_{1/2}Ti_{1/2})O_3$-x$PbTiO_3$ ceramics, the phase fraction of the coexisting monoclinic and tetragonal phases changes by changing grain size [Upadhyay and Singh (2017)].

The Rietveld fits for pseudocubic (110), (111), and (200) XRD profiles of the samples prepared at different temperatures reported by Upadhyay and Singh (2017) considering coexistence of tetragonal and monoclinic structures are shown in **Fig. 1.18**. Variation of monoclinic phase fraction with heat treatment temperature for 0.65$Bi(Mg_{1/2}Ti_{1/2})O_3$-0.35$PbTiO_3$ ceramic is shown in **Fig. 1.19**. It is reported that monoclinic phase fraction decreases with the increase in the heat treatment temperature while the tetragonal phase get more stabilized on increasing the heat treatment temperature (see **Fig. 1.19**).

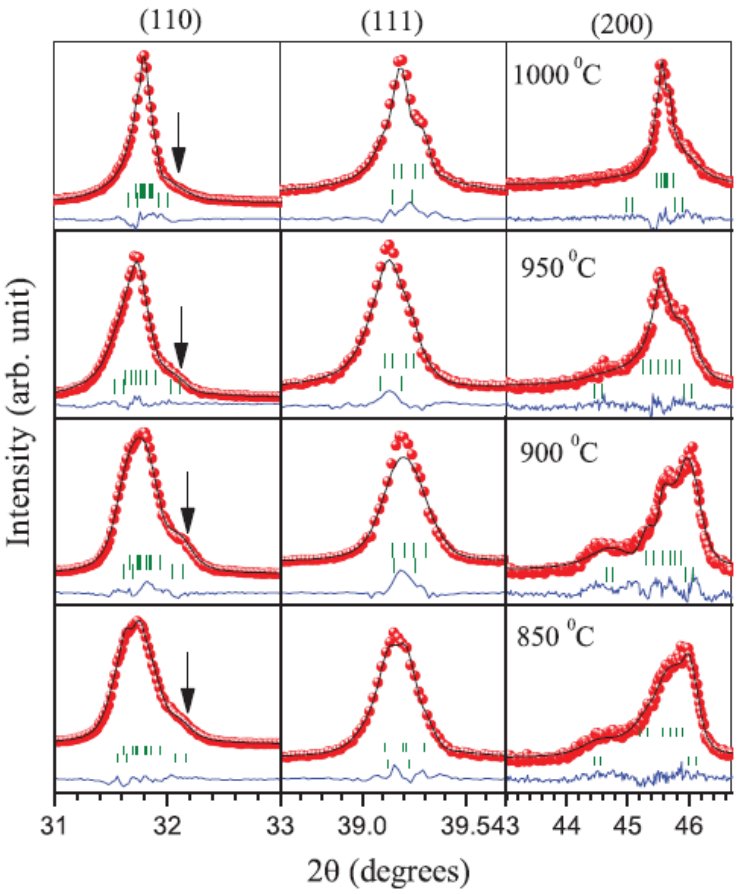

Figure 1.18 Experimentally observed (dots), Rietveld calculated (continuous line, and their difference (continuous bottom line) profiles for pseudocubic (110), (111) and (200) reflections obtained after Rietveld analysis of XRD data for $0.65Bi(Mg_{1/2}Ti_{1/2})O_3$-$0.35PbTiO_3$ using coexistence monoclinic + tetragonal (Pm-P4mm) structures for various heat treatment temperatures. The vertical tick marks above the bottom line show peak position [After Upadhyay and Singh (2015)].

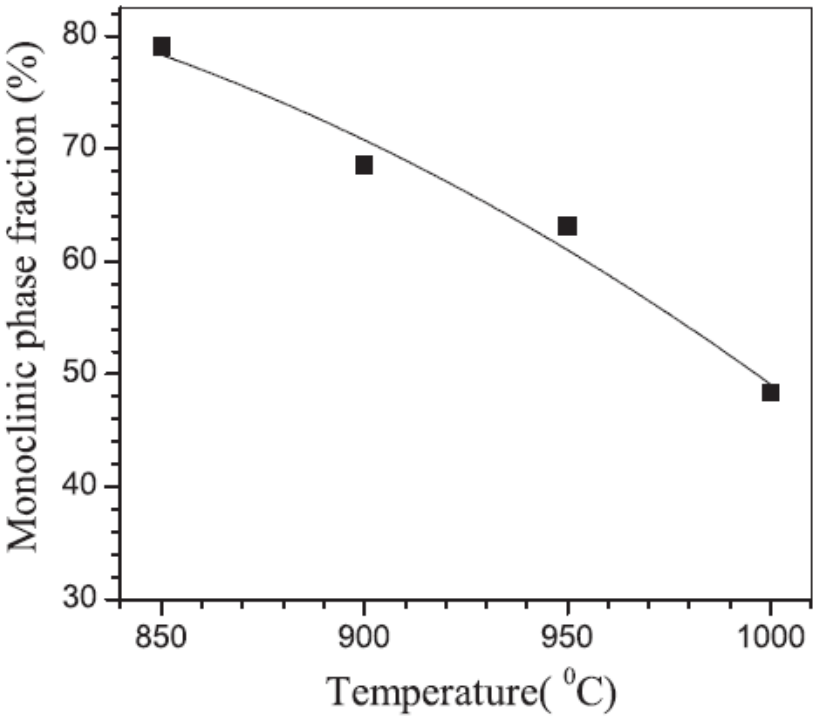

Figure 1.19 Variation of monoclinic phase fraction with increasing heat treatment for $0.65Bi(Mg_{1/2}Ti_{1/2})O_3$-$0.35PbTiO_3$ [Upadhyay and Singh (2015)].

The lattice parameters of two coexisting phases are also reported to get modified by changing the grain size. The variation of lattice parameters of $0.65Bi(Mg_{1/2}Ti_{1/2})O_3$-$0.35PbTiO_3$ piezoceramic with heat treatment temperature reported by Upadhyay and Singh (2015) is shown in **Fig. 1.20**. One can clearly see significant modification in the tetragonal c-parameter by changing the grain size.

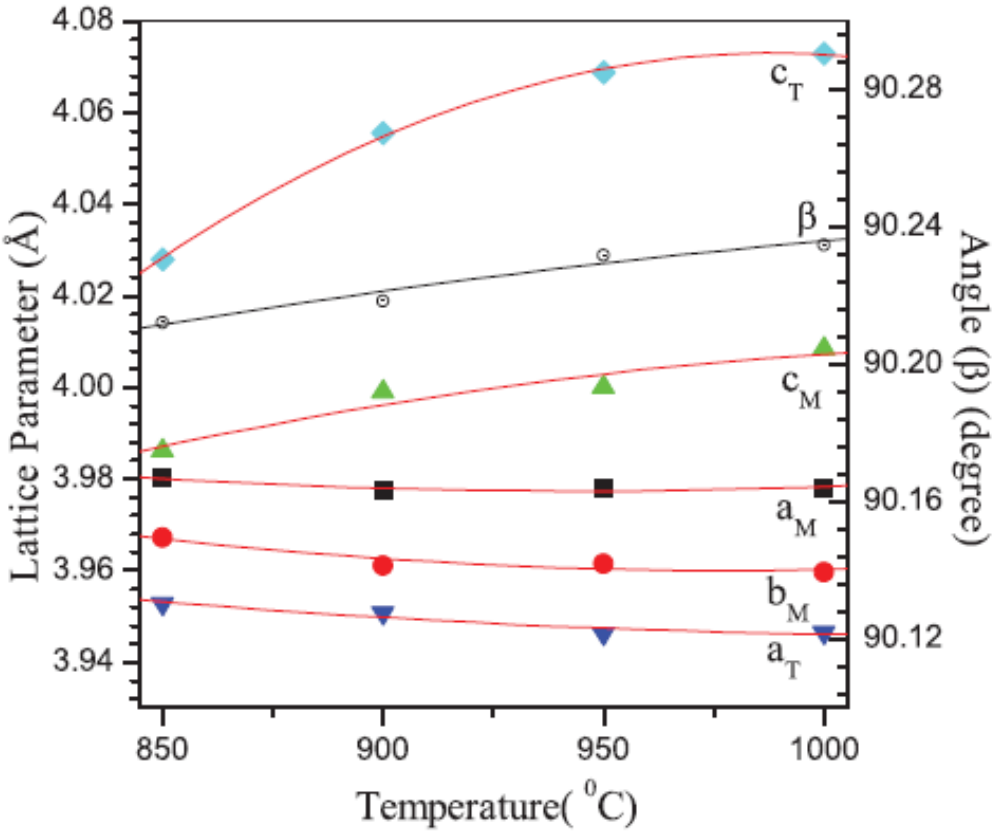

Figure 1.20 Variation of lattice parameters with increasing heat treatment temperature (increased grain size) for $0.65Bi(Mg_{1/2}Ti_{1/2})O_3$-$0.35PbTiO_3$ [Upadhyay and Singh (2015)].

Investigation of the microstructure of $0.65Bi(Mg_{1/2}Ti_{1/2})O_3$-$0.35PbTiO_3$ samples prepared at various heat treatment temperatures confirms that the grain size increases with increasing preparation temperature. The SEM micrograph of $0.65Bi(Mg_{1/2}Ti_{1/2})O_3$-$0.35PbTiO_3$ ceramic taken after the heat treatment at four different temperatures, 850°C, 900°C, 950°C and 1000°C reported by Upadhyay and Singh (2015) is shown in **Fig. 1.21**. The grain size is seen to increase with the increase of heat treatment temperature. The grain size was reported as 200, 400, 500 and 1000 nm for the samples heat treated at

temperatures 850°C, 900°C, 950°C and 1000°C, respectively [Upadhyay and Singh (2015)]. Thus, the grain size effects in MPB ceramics needs to be properly understood.

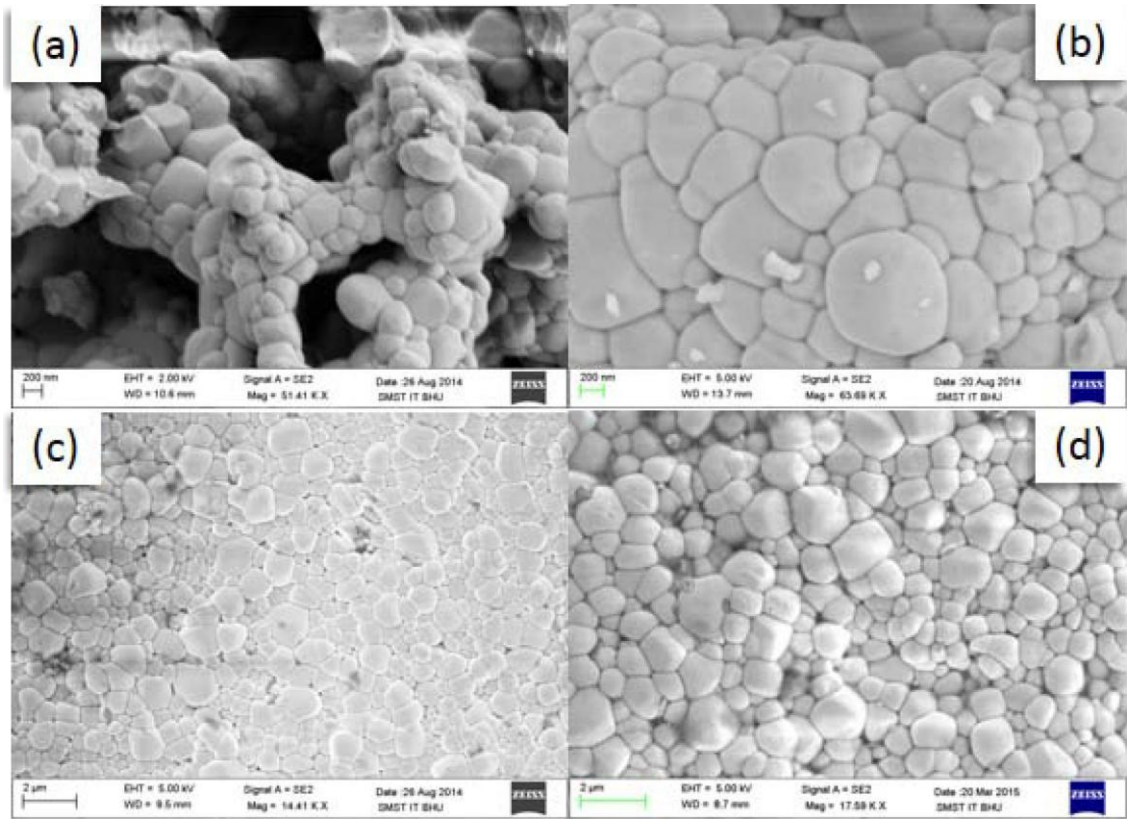

Figure 1.21 SEM images of $0.65Bi(Mg_{1/2}Ti_{1/2})O_3$-$0.35PbTiO_3$ ceramics prepared at 850°C, 900°C, 950°C and 1000°C temperatures [After Upadhyay and Singh (2015)].

1.18 Objectives of the Present Thesis Work

It is evident from the foregoing review that the room temperature crystal structure and location of the morphotropic phase boundary compositions in $(1-x)Bi(Mg_{3/4}W_{1/4})O_3$-$xPbTiO_3$ ceramic is not studied properly. No detailed structural investigation has been done on this system. Further, a systematic temperature dependent crystal structure and phase studies for various compositions across MPB is also lacking. Structural investigations after

electric field poling of the MPB compositions of (1-x)Bi($Mg_{3/4}W_{1/4}$)O_3-x$PbTiO_3$ ceramic are also not done so far. There is no report on the effect of grain size on the crystal structure and phase coexistence in the MPB compositions of this system. In view of the above, we set following important objectives of the present thesis work:

1. To synthesize pure perovskite phase of (1-x)Bi($Mg_{3/4}W_{1/4}$)O_3-x$PbTiO_3$ solid solution.
2. To study the room temperature crystal structure of (1-x)Bi($Mg_{3/4}W_{1/4}$)O_3-x$PbTiO_3$ solid solution across the morphotropic phase boundary and determine the phase coexistence region at room temperature by Rietveld structural analysis.
3. To investigate the composition and temperature dependent structural phase transition in (1-x)Bi($Mg_{3/4}W_{1/4}$)O_3-x$PbTiO_3$ ceramics.
4. To investigate the composition and temperature dependent dielectric behaviour of (1-x)Bi($Mg_{3/4}W_{1/4}$)O_3-x$PbTiO_3$ ceramics.
5. To investigate the electric field induced structural phase transitions in (1-x)Bi($Mg_{3/4}W_{1/4}$)O_3-x$PbTiO_3$ ceramics.
6. To investigate the effect of the off-stoichiometry on the crystal structure and dielectric behaviour of (1-x)Bi($Mg_{3/4}W_{1/4}$)O_3-x$PbTiO_3$ ceramics.
7. To investigate the grain size dependent structural transformations in the MPB composition of (1-x)Bi($Mg_{3/4}W_{1/4}$)O_3-x$PbTiO_3$ ceramics.